Recent Advances in Hybrid Molecular Imaging Systems

Jae Sung Lee, PhD[1] Joong Hyun Kim, PhD[2]

[1] Departments of Nuclear Medicine and Biomedical Sciences, Seoul National University College of Medicine, Seoul, Korea
[2] Department of Nuclear Medicine, Seoul National University Bundang Hospital, Gyeonggi-Do, Korea

Address for correspondence Jae Sung Lee, PhD, Department of Nuclear Medicine, Seoul National University College of Medicine, 28 Yungun-Dong, Chongno-Gu, Seoul 110-744, Korea (e-mail: jaes@snu.ac.kr).

Semin Musculoskelet Radiol 2014;18:103–122.

Abstract

Nuclear medicine imaging methods that use radionuclides, such as positron emission tomography (PET) and single-photon emission computed tomography (SPECT), offer highly sensitive and quantitative tools for the detection and localization of the biochemical and functional abnormalities associated with various diseases. The introduction of dual-modality PET/CT and SPECT/CT systems to the clinical environment in the late 1990s is regarded as a revolutionary advance in modern diagnostic imaging, bringing precise anatomical localization to conventional PET and SPECT imaging techniques and enhancing the quantitation capabilities of these modalities. The great success of PET/CT has also revived interest in the combination of PET and MR scanners, leading to commercially available clinical PET/MR systems. In this article, we review the recent improvements made in these hybrid molecular imaging systems, which have been dramatic in terms of both hardware and software over the past decade. We focus primarily on the hybrid imaging systems that are currently used in clinical practice and the technologies applied in those systems, with emphasis on the efforts to improve their diagnostic performances for musculoskeletal diseases.

Keywords
- PET/CT
- SPECT/CT
- PET/MR
- hybrid imaging

Imaging is an indispensable tool in modern medicine. The revolutionary invention of tomographic imaging technologies in the 1970s and 1980s and the continuing innovation in these technologies over the last few decades has substantially improved diagnostic capabilities for many human diseases. X-ray computed tomography (CT), which produces an image from X-ray attenuation, has experienced remarkable technological advancements in both hardware design and software algorithms in recent years (e.g., multislice and volumetric CT and various low-dose solutions).[1–3] MRI has become firmly established as a preferred diagnostic imaging tool following the substantial improvements made in both scan speed and image quality since its introduction to clinical practice in the early 1980s.[4–6]

Nuclear medicine imaging methods that use radionuclides, such as positron emission tomography (PET) and single-photon emission computed tomography (SPECT), offer highly sensitive and quantitative tools for the detection and localization of the biochemical and functional abnormalities associated with various diseases. In addition, molecular imaging techniques based on radionuclide imaging are the most sensitive methods that are readily translatable to clinical use.[7] However, the major drawbacks of stand-alone PET and SPECT systems are their relatively poor spatial resolutions and low signal-to-noise ratios. The absence of background anatomical information in stand-alone PET and SPECT images of highly target-specific radiotracers sometimes make it difficult to interpret the distributions of these tracers. To overcome these limitations of PET and SPECT, many algorithms and software solutions for retrospective coregistration and fusion of PET and SPECT images with the morphological images provided by CT and MRI have been developed.[8–11] However, their use was limited in normal clinical settings, mainly because additional efforts are required to retrieve and

Issue Theme Update in Musculoskeletal Hybrid Imaging; Guest Editor, Seoung-Oh Yang, MD, PhD

DOI http://dx.doi.org/10.1055/s-0034-1371014.
ISSN 1089-7860.

process the image data and because most human organs and soft tissues have a deformable nature that could lead to image mismatch.

The introduction of dual-modality PET/CT and SPECT/CT systems in the late 1990s, in which PET and SPECT are combined with X-ray CT in a clinical setting, is regarded as a revolutionary advance in modern diagnostic imaging. In these systems, the PET or SPECT images are acquired sequentially with the CT images using a single device and without moving the patient from the bed, eliminating differences in patient positioning and minimizing the misalignments caused by internal organ motion.[12–16] The anatomical information provided by the CT images enhances the user's confidence in the PET and SPECT findings. Additionally, the attenuation map derived from the X-ray CT for the gamma rays emitted from the radionuclides offers useful ways to correct for the attenuation and scatter artifacts in PET and SPECT with minimal addition to the scan time and the image noise.[16–18]

The concept of simultaneous acquisition of PET and MR images was also suggested in the early days of dual-modality systems development, and the development of PET/MR scanners started in the 1990s.[19,20] However, progress in the development process was relatively slow, and the realization of clinical PET/MR scanners was greatly delayed because of technical difficulties when operating PET and MR scanners in close proximity combined with a lack of industrial interest and concern over the high cost of the combined device.[21] The great success of nuclear medicine imaging modalities when combined with CT has, however, revived interest in the combination of PET and MR scanners. The technical advances made over the long development period to minimize the mutual interference between the PET and MR data acquisition processes have led to combined clinical PET/MR scanners with sequential and simultaneous imaging strategies in recent years. The major advantages of PET/MR include a smaller radiation burden than PET/CT, better soft tissue contrast when using MRI rather than CT, and possible simultaneous acquisition of images.

This article reviews the recent advances in hybrid medical imaging systems. In this review, we focus primarily on the hybrid imaging systems that are currently available for clinical practice and the technologies applied in those systems. In each section, the basic principles, fields of application, and recent advances are reviewed for each hybrid imaging device. It should be noted that most of the technical advances in each of the components of the hybrid imaging systems are also available for the stand-alone nuclear medicine and radiologic imaging systems because the overall performance of each hybrid imaging system is a function of the performance of the individual components. Although the applications of most of the technologies introduced in this article are not limited to musculoskeletal imaging, we emphasize the efforts made to improve the diagnostic performances for musculoskeletal diseases.

Advances in SPECT/CT

Basic Principles, Advantages, and Applications

SPECT has several advantages over PET, including greater accessibility, lower cost, and better availability of radiotracers for the investigation of a wider range of biological processes.[22] Technetium 99m (^{99m}Tc) is the most widely used radioisotope in SPECT; it has a 6-hour half-life and is simply produced using a molybdenum 99 (^{99}Mo)/^{99m}Tc generator. The local production of many SPECT radiotracers is also possible using commercially available kits. Other radioisotopes used in SPECT include gallium 67 (^{67}Ga), indium 111 (^{111}In), iodine 123 (^{123}I), and iodine 131 (^{131}I). Because these radioisotopes emit gamma rays with different energies, simultaneous data acquisition using dual or multiple radioisotopes is possible in principle. ^{99m}Tc-labeled phosphate-containing compounds, such as ^{99m}Tc-methylenediphosphonate (^{99m}Tc-MDP) and ^{99m}Tc-hydroxydiphosphonate (^{99m}Tc-HDP), are the most widely used radiotracers for bone imaging (►**Fig. 1**). In the diagnosis of musculoskeletal infection, ^{99m}Tc-dicarboxypropane diphosphonate (^{99m}Tc-DPD), ^{67}Ga, ^{111}In-labeled leukocytes, and ^{99m}Tc-labeled antigranulocyte antibodies are used.[23]

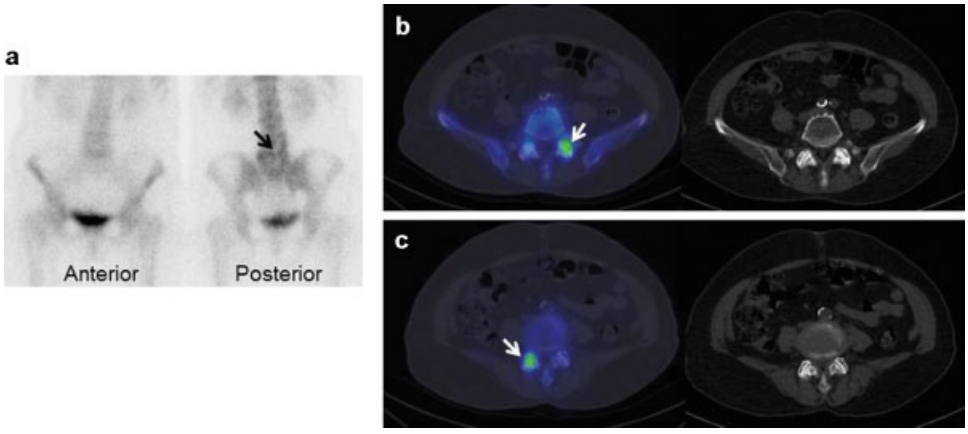

Fig. 1 A 76-year-old female patient who experienced lower back pain underwent bone scan and SPECT/CT imaging after injection of ^{99m}Tc-MDP to find the focus of active lesion. (**a**) On bone scan, a focal increased uptake was found in the left side of the L4–L5 intervertebral area. (**b**) On SPECT/CT, however, the focal uptake was revealed to be on the right facet joint of L4–L5. (**c**) In addition, a focal uptake was also found on the left facet joint of L3–L4 that was not noticed on the bone scan.

Basic Principles and Design of SPECT Systems

In SPECT imaging, single-, dual- or triple-headed gamma cameras attached to a rotating gantry are used for angular data sampling. The projection data are acquired in either step-and-shoot mode or continuous mode, and they are rearranged into multiple sinograms for tomographic image reconstruction. The gamma cameras (or SPECT detectors) consist of a collimator and a position-sensitive radiation detector. The collimator is made from heavy radiation shielding material and used to reject gamma-ray photons that are not within the desired incidence angle for each angular position of the gamma camera. In general, there is a trade-off between resolution and sensitivity in the collimator selection process because the collimators used for high-resolution imaging yield low sensitivities because of their low geometric efficiency. The radiation detector conventionally used in gamma cameras is the scintillation detector, which indirectly converts radiation into electronic signals. In the scintillation detector used for SPECT, a large-area continuous NaI(Tl) scintillation crystal is coupled to an array of photomultipliers (PMTs) via a light guide. The visible light photons generated in the scintillation crystal by the gamma-ray interaction are read by the PMT array arranged in a hexagonal pattern to obtain energy and position information for each gamma-ray interaction.

Advances in Conventional SPECT Detectors

In most modern SPECT detectors based on NaI(Tl) crystals and PMTs, most of the electronics, including the front-end analog circuit and the analog-to-digital (ADC) converters, are mounted directly on the individual PMTs to minimize signal distortion in the long signal readout cables.[24,25] These digitized detectors enable calculation of the gamma-ray interaction position and energy and the elimination of pulse pileups in the software with more sophisticated algorithms than those used for conventional analog circuit-based approaches.[26,27] In modern gamma cameras, only PMTs with output signals above a certain threshold are included in the position and energy calculations. The main purposes of this signal thresholding process are to suppress noisy signals from the PMTs and to allow only the output signals from the small number of PMTs around the gamma-ray interaction position to be used in the position and energy calculations. By restricting the number of PMTs used, the multiple events that occur in different positions in a continuous NaI(Tl) crystal can be recorded simultaneously.[25,28] The modern gamma cameras with these advanced hardware technologies yield $\sim$ 10% full width at half maximum (FWHM) energy resolution for ^{99m}Tc and $\sim$ 2- to 4-mm FWHM spatial resolution. Event rates of up to 10^5 per second are typically supported.[29]

Solid-state SPECT and SPECT/CT

One of the most important emerging technologies in SPECT is the use of cadmium zinc telluride (CZT) semiconductor gamma-ray detectors. Because the CZT converts the gamma rays into electric signals directly, the spatial and energy resolutions of this detector are better than those of conventional NaI(Tl)-based indirect detectors. The intrinsic spatial resolution of current CZT detectors is $\sim$ 2.5 mm, which is independent of the gamma-ray energy.[30] The higher energy resolution of the CZT detector provides improved performance in terms of rejection of scatter and cross talk gamma-ray photons during multiple-tracer imaging. Two vendors now provide cardiac-dedicated CZT SPECT and SPECT/CT systems. The cardiac-dedicated CZT SPECT system of Spectrum Dynamics (now acquired by Biosensors International Group) contains nine independently rotating CZT detector modules that are equipped with a parallel-hole collimator.[31,32] GE Healthcare has combined CZT detectors with a multi-pinhole collimator, enabling simultaneous multiple-tracer imaging and stationary data acquisition without rotation of the gamma camera (►**Fig. 2**).[33,34] Garcia et al showed that the spatial resolution and sensitivity have been improved by two and six times, respectively, when compared with the

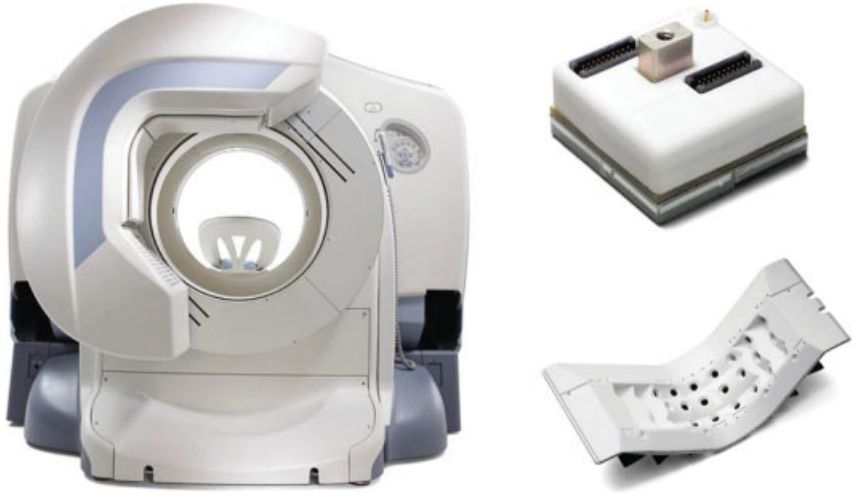

Fig. 2 Cadmium zinc telluride (CZT)-based cardiac hybrid SPECT/CT scanner (NM/CT 570c) and CZT detector and multi-pinhole collimator used in this system. (Image courtesy of GE Healthcare.)

properties of conventional NaI(Tl)-based cameras.[35] Although the application of this innovative semiconductor detector technology is mainly limited to cardiac-dedicated SPECT and SPECT/CT systems because of the cost, the commercial production of general-purpose scanners based on this technology is expected in the near future.

Advances in Filtering and Reconstruction Technologies

One of the most remarkable recent improvements in gamma camera and SPECT software is the widespread application of smoothing filters with variant kernel sizes that are adaptive to the anatomical details of each region. The smoothness of the post-filtered image is determined by the cutoff frequency (in the frequency domain) or the kernel size (in the spatial domain) of the smoothing filter. A lower cutoff frequency or a wider kernel size in the smoothing filter leads to a more blurred post-filtered image. In nuclear medicine, linear space invariant filters, such as Butterworth, Hanning, Wiener, Metz, and Gaussian filters, have conventionally been used because fast generation of the filtered images is made possible by the convolution integration of the images with the fixed filter kernel when the kernel parameters are determined. However, the desired or optimal kernel size for medical images would not be spatially invariant or uniform because the anatomical variation or detail varies depending on both the organ and the location. Therefore, the kernel size of the smoothing filters that are currently used in the "half-time solution" of each vendor is adaptively adjusted for each pixel based on the similarities of the pixel values with those of the surrounding pixels. Filters with wider kernels are applied to areas with a relatively uniform pixel count to fully suppress the noise; filters with narrower kernels are applied to areas with high count variability to preserve the edge information. ►**Fig. 3** shows that the quality of a bone scan image acquired in half time and processed with this type of adaptive filter is equivalent to that of a conventional image acquired in standard time.

The incorporation of the collimator-detector response (CDR) in the iterative image reconstruction process is also useful for both noise reduction and improved spatial resolution. A projection image of a point source is used as a measure of blurring and referred to as the CDR in gamma cameras.[36] The CDR of a gamma camera is determined by several factors including the distance of the point source from the gamma camera, the shape and geometry of the collimator, the dimensions and properties of the scintillation crystal, and the scintillation light sharing and collection method. The four main components of the CDR are the intrinsic response, the geometric response, the septal penetration, and the septal scatter.[36–38] The distance dependence of the CDR mainly originates from the geometric response of the collimator, which is determined by the acceptance angle for the incident gamma rays. The rapidly increasing computation speeds and parallel computing capabilities of modern computers allow the popular use of iterative statistical reconstruction methods for SPECT, in which the CDR and other physical factors (i.e., attenuation and scattering) are incorporated to achieve higher image quality. ►**Fig. 4** shows that this type of CDR

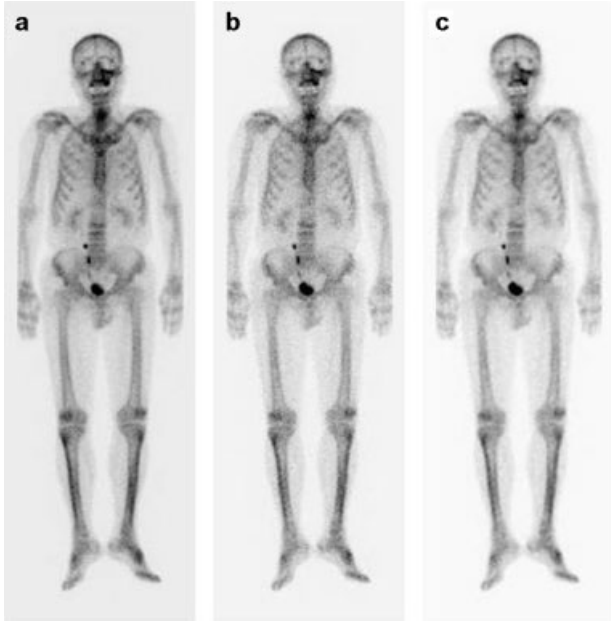

Fig. 3 ^{99m}Tc-MDP bone scintigraphic images acquired (**a**) for standard scan time without applying adaptive filter, (**b**) half time without filter, and (c) half time with filter.

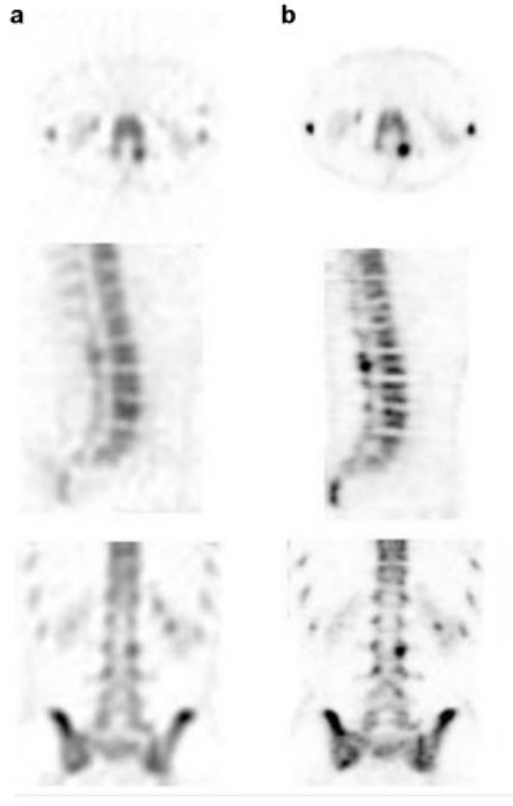

Fig. 4 ^{99m}Tc-MDP SPECT images in a patient with presumptive pars interarticularis stress in a spine reconstructed using (**a**) conventional filtered back projection method and (**b**) iterative ordered subset expectation maximization method with distant-dependent collimator-detector response modeling for resolution recovery. (Reprinted from Stansfield et al[39] with permission.)

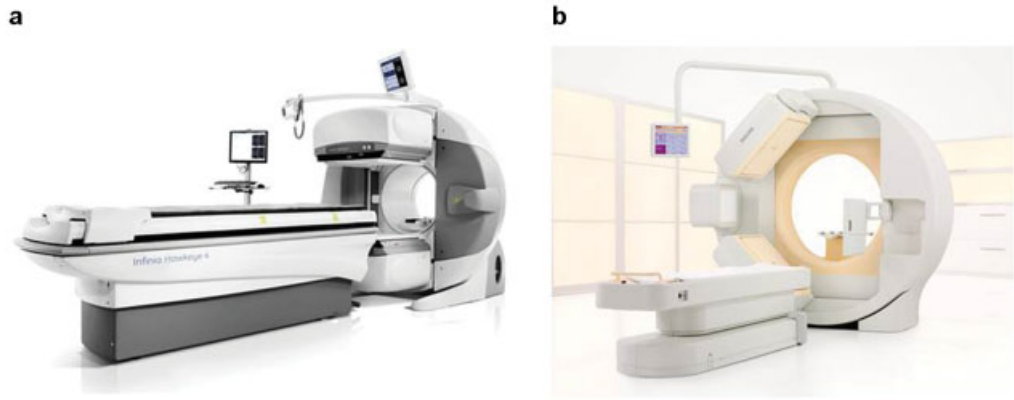

Fig. 5 SPECT/CT systems with a low-cost cone-beam CT based on a flat panel X-ray detector and a low-power X-ray tube mounted on the same gantry as the SPECT system. (**a**) GE Infinia Hawkeye. (**b**) Philips BrightView XCT. (Image courtesy of GE Healthcare and Philips Healthcare.)

modeling-based iterative reconstruction enhances image quality by improving image sharpness and the ability to detect lesions when compared with conventional filtered back projection (FBP) reconstruction.[39]

Trends in SPECT/CT Systems

The use of hybrid SPECT/CT as a diagnostic modality has been gradually increasing since the first commercial SPECT/CT was launched in 1999. Current SPECT/CT scanners typically consist of a dual-head SPECT system combined with a CT system.[25] Two types of CT systems are now used in SPECT/CT. The first type is a low-cost cone-beam CT based on a flat panel X-ray detector and a low-power X-ray tube mounted on the same gantry as the SPECT system (e.g., GE Infinia Hawkeye and Philips BrightView XCT systems) (►**Fig. 5**). The CT rotation speed is slower than that of state-of-the-art multidetector CT (MDCT) systems. Although the morphological detail is not compatible with diagnostic quality MDCT, the images obtained using the cone-beam CT address the needs of the SPECT attenuation correction and anatomical localization processes well. The second type is a fast-rotating MDCT system combined in tandem with the SPECT system (►**Fig. 6**). These systems (e.g., Siemens Symbia and GE Discovery NM/CT 670 systems) offer diagnostic CT image quality that is especially suitable for oncologic and musculoskeletal studies and has a sufficiently fast scan speed for applications that require intravenous iodine contrast enhancement.[14,23]

Improved SPECT Quantification

The quantitative accuracy of SPECT images has been greatly increased by incorporation of CT information in the SPECT reconstruction.[40] In addition to the resolution recovery produced by incorporating the CDR in the image reconstruction process, correction for gamma-ray attenuation is the most important process for accurate quantification of the radioactivity in SPECT. Previous approaches used for attenuation correction in stand-alone SPECT using radioisotope transmission sources (e.g., ^{153}Gd, ^{99m}Tc, and barium 133 [^{133}Ba]) required long scan times and yielded poor signal-to-noise ratios.[38,41,42] In SPECT/CT, converted attenuation maps for SPECT from the Hounsfield units of the high-quality CT images are now routinely used for attenuation correction. ►**Fig. 7** shows the improved quantitative accuracy of modern SPECT images that is compatible to the PET.

The CT information can also be used for context-specific SPECT reconstruction that enhances the effective image

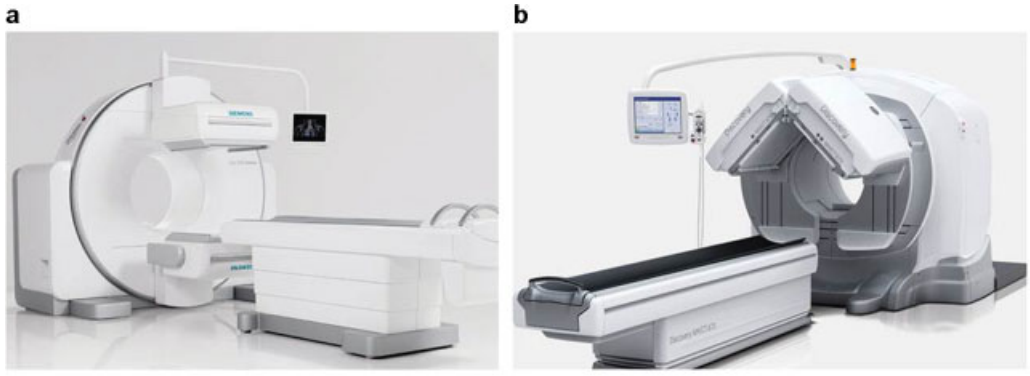

Fig. 6 SPECT/CT systems with a fast-rotating MDCT system combined in tandem with the SPECT system. (**a**) Siemens Symbia Intevo. (**b**) GE Discovery NM/CT 670. (Image courtesy of Siemens Healthcare and GE Healthcare.)

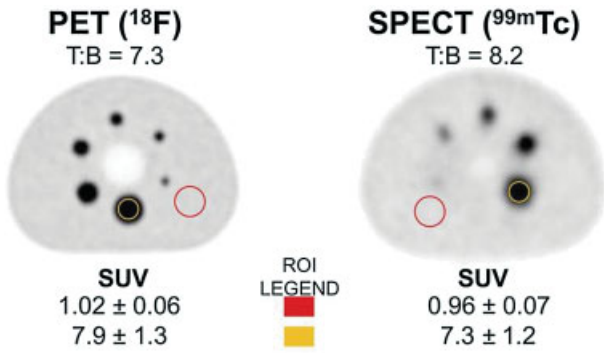

Fig. 7 An example comparing the quantitative accuracy of PET and SPECT images expressed as standard uptake value (SUV). ROI, region of interest. (Reprinted from Bailey and Willowson[40] with permission.)

quality of the spatial resolution of the SPECT images. In the new context-specific reconstruction method for bone SPECT/CT recently introduced by Siemens Healthcare, the CT pixels were divided into five tissue classes ("zones": air and lung, adipose, soft tissue, soft bone, and cortical bone) with smooth boundaries based on their intensities. Zonal images are then forward projected to create zonal data models; the weighted sum of these models is compared with the measured projection data, and the error occurring between them is back-projected to update the reconstructed SPECT image. This procedure is repeated until the stopping criterion is reached. As shown in ►**Fig. 8**, the boundaries of the different tissue classes are well resolved as delineated in CT, but the resolution inside each class is similar to that of a conventional SPECT image.[43]

Advances in PET/CT

Basic Principles, Advantages, and Applications

The nuclei of the radioisotopes used in PET have relatively small numbers of neutrons in comparison with those of stable isotopes. Thus one of the protons inside the radioisotope is converted into a neutron while releasing a positron, which is the antiparticle of an electron with the opposite charge. The mutual annihilation of this positron and an electron results in the simultaneous emission of a pair of annihilation (gamma-ray) photons with identical energies (511 keV) but in opposite directions. The radioisotope most widely used in PET is fluorine 18 (^{18}F), which has a ~ 110-minute half-life and is produced using a cyclotron. Because of the relatively long half-life of ^{18}F, the radiopharmaceuticals labeled with ^{18}F at one location can be provided to the other imaging centers. Other PET radioisotopes include carbon 11 (^{11}C), nitrogen 13 (^{13}N), oxygen 15 (^{15}O), rubidium 82 (^{82}Rb), ^{68}Ga, and ^{124}I.

The improved spatial resolution, fast whole-body imaging capability, and anatomical CT information of modern PET/CT scanners contribute to the improved diagnostic performance of PET/CT examinations for various musculoskeletal disorders (►**Fig. 9**). In particular, the misinterpretation of benign lesions with increased ^{18}F-FDG uptake as malignant processes can be reduced by evaluation of the bone on the CT portion of the musculoskeletal PET/CT examination.[44] There is therefore increasing evidence in the literature to support the incremental benefits of using PET/CT in the diagnosis of musculoskeletal malignancies along with conventional anatomical imaging modalities.[45]

When compared with conventional whole-body bone scintigraphy using ^{99m}Tc-labeled phosphates, bone PET and PET/CT imaging with ^{18}F-fluoride offer several advantages including faster and higher bone uptake, faster blood clearance, and greater in vivo stability.[46,47] Thus lower uptake times are required for static bone imaging (15–30 minutes as compared with 3–4 hours for ^{99m}Tc-MDP), which results in more efficient workflows and provides greater comfort to patients.[46,48] The superior spatial resolution and higher sensitivity of PET scanners when compared with gamma cameras also contribute to the higher diagnostic accuracy in the assessment of malignant and benign skeletal diseases when using ^{18}F-fluoride.[48,49] ►**Fig. 10** shows an example of focally increased uptake demonstrated on ^{18}F-fluoride PET/CT but not on ^{18}F-FDG PET/CT in a patient with an osteolytic metastatic lesion in pelvic bone. Although ^{18}F-fluoride has not been widely used in clinical practice, mainly because of the greater availability of ^{99m}Tc-labeled phosphates, a global shortage of ^{99m}Tc and the increased availability of PET and hybrid imaging systems are provoking greater interest in the role of ^{18}F-fluoride in clinical bone imaging applications.

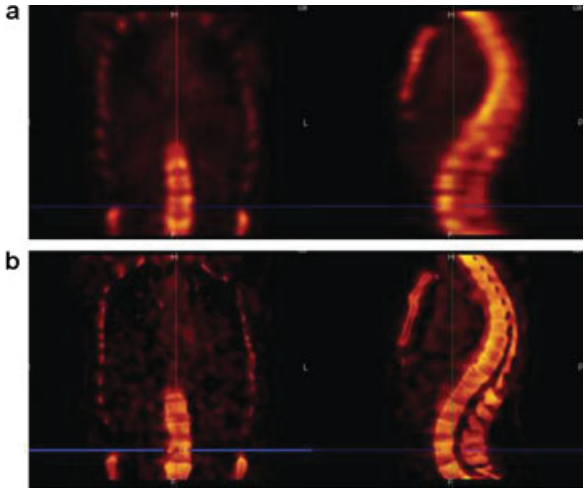

Fig. 8 Comparison of ^{99m}Tc-MDP bone SPECT images obtained using (**a**) conventional iterative reconstruction with resolution recovery and (**b**) context-specific reconstruction. (Reprinted from Vija[43] with permission.)

PET Scintillation Crystals

Scintillation detectors are also used in PET scanners to measure the gamma-ray photons. However, no mechanical collimator is required in PET, in contrast to the gamma cameras, because coincidence detection of the gamma-ray pairs flying in 180-degree opposite directions provides the location of their origin along a line (the so-called line of response [LOR]) between the two PET detectors. Thus PET scanners with multiple scintillation detector rings have higher sensitivity than gamma cameras, in which most of the gamma rays are absorbed by the collimator. Because

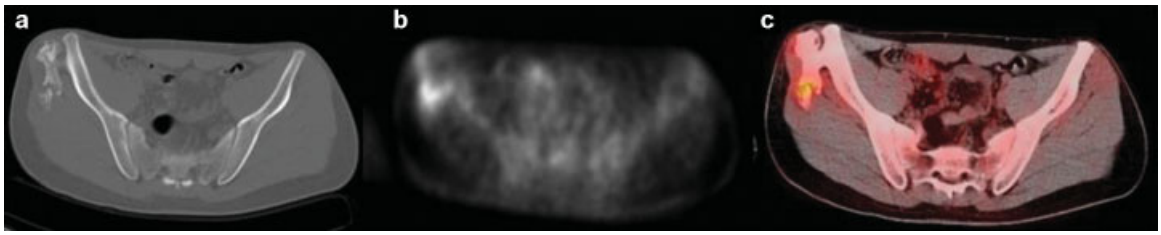

Fig. 9 A 19-year-old male patient who was alleged to have a bone tumor in the right pelvic area underwent ^{18}F-FDG PET/CT imaging to characterize the tumor. (**a**) On CT imaging, a bone-forming mass was found on the right side of the right iliac wing. (**b, c**) On PET and PET/CT images, mild FDG uptake (standard uptake value [SUV]max: 3.1) was found only on the posterior part of the mass. Considering the morphology and the degree of FDG uptake, the mass was judged to be a benign osteochondroma without sarcomatous change, and the biopsy result concurred with the conclusion from the imaging finding.

accurate coincidence detection of the gamma-ray pairs with much higher energies (511 keV compared with 140-keV gamma rays from ^{99m}Tc) is an essential process in PET scanners, the scintillation crystals used in the PET detectors should be sufficiently bright, fast, heavy, and dense. In modern PET and PET/CT scanners, arrays of segmented cerium-doped lutetium (Lu)-based crystals (i.e., LSO, LYSO, and LGSO) are commonly used as alternatives to the conventional BGO crystals with their slow decay times because of their excellent physical properties.

In recent years, smaller size crystal elements (~ 4 mm $\times$ 4 mm) and higher numbers of detectors along the axial direction (20–25 cm) have been used to improve the spatial resolution and sensitivity of clinical PET scanners. PET detectors with depth-of-interaction measurement capabilities have also been investigated in depth but have not yet been applied to clinical PET scanners.[50,51] ►**Fig. 11** shows the representative PET/CT systems from the major vendors.

Time-of-Flight PET

Another important trend in clinical PET hardware systems is the improvement in the detectors and associated electronics technologies that are used to measure the time-of-flight (TOF).[18,25] TOF measurements in PET (i.e., measurement of the arrival time difference between two annihilation photons) allow us to restrict the annihilation position probability to a small segment of interest during the back-projection procedure in image reconstruction. Therefore, we can use this TOF information to reduce the noise generated during image reconstruction, as shown in ►**Fig. 12**. The reduction in background noise provided by the TOF information allows better lesion detectability, as shown in ►**Fig. 13**, in which the non-TOF PET and TOF PET images were compared.[52] The benefit of the TOF information is even more remarkable in low-statistics images, indicating that this technique is useful for reducing the PET scan time or even the radiopharmaceutical injection dose. Further improvements in image quality

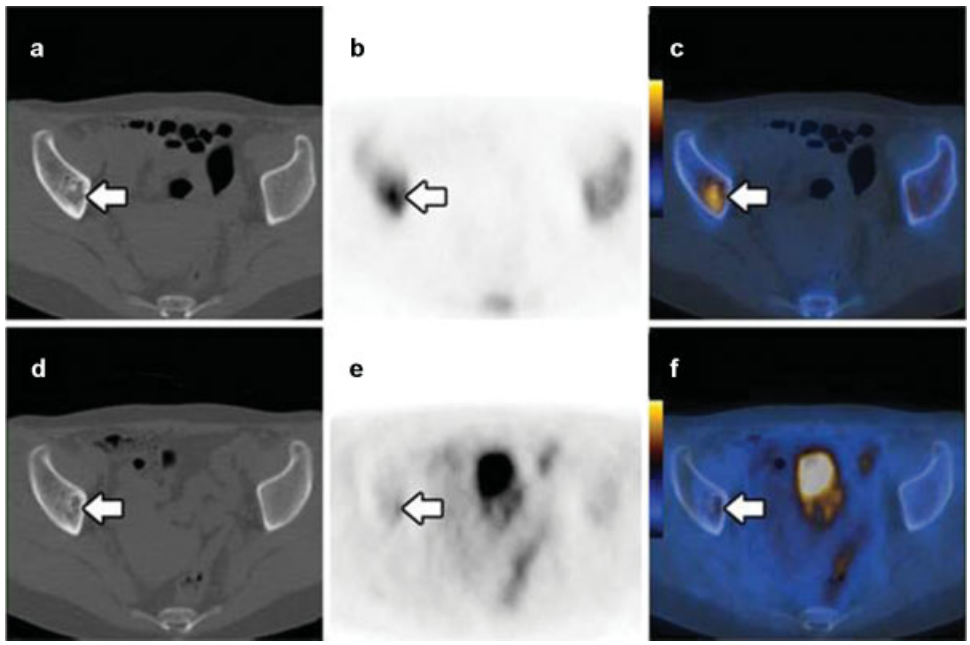

Fig. 10 Osteolytic metastatic lesion in pelvic bone (arrow). Focally increased uptake was demonstrated on ^{18}F-fluoride PET/CT (**a**, CT; **b**, PET; **c**, fused PET/CT image), but not on ^{18}F-FDG PET/CT (**d**, CT; **e**, PET; **f**, fused PET/CT image). (Reprinted from Yoon et al[47] with permission.)

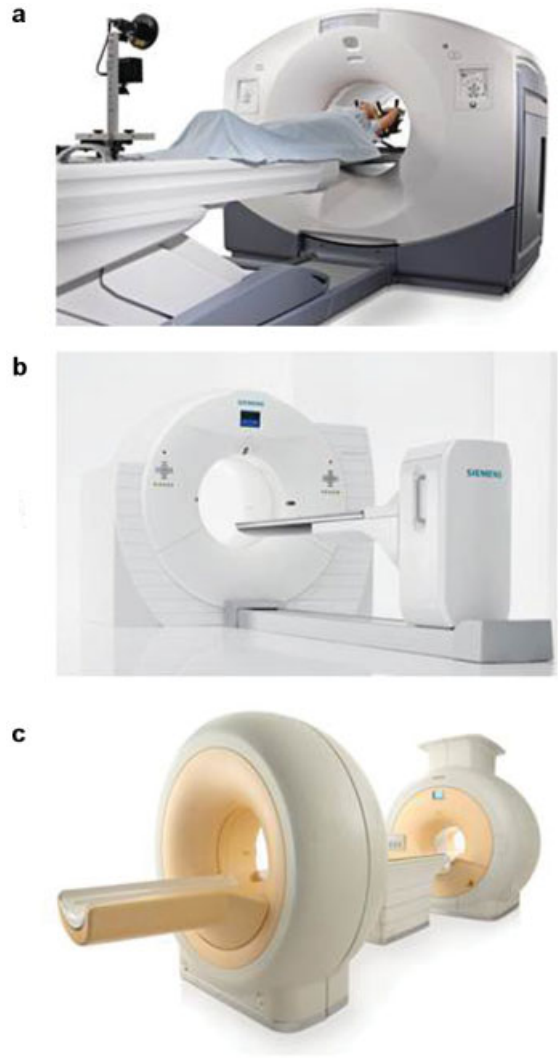

Fig. 11 Representative PET/CT systems from the major vendors. (**a**) GE Discovery PET/CT 710. (**b**) Siemens Biograph mCT Flow. (**c**) Philips Ingenuity TF. (Image courtesy of GE Healthcare, Siemens Healthcare, and Philips Healthcare.)

can be achieved because of the better timing resolution of the PET scanners. In ►**Fig. 14**, the images in the middle columns are taken from the current generation of PET scanners with 600 ps coincidence timing resolution; the image on the right is from a potential next-generation scanner with 300 ps timing resolution. Faster contrast recovery for small lesions is another benefit offered by the TOF PET with its higher timing.[52]

Resolution Modeling in PET

Incorporation of resolution degradation factors within the system matrix (whose elements model the relationship between the object and the projection space) used for iterative reconstruction also contributes to the improvement in PET image quality.[18,53] These resolution degradation factors include the positron range, the annihilation photon acollinearity, and the intrinsic detector resolution. Spatially variant resolution modeling results in increased computational complexity but provides optimal reconstruction results by taking the nonuniform resolution of the PET scanner in both radial and axial locations into account. This resolution modeling in PET provides improved image reconstruction in terms of both spatial resolution and image contrast.[54] The combination of resolution modeling and the TOF information in the image reconstruction process provides higher image quality and better lesion detectability than that provided by the singular use of these technologies (►**Fig. 15**).[53,55–57] It should be noted, however, that resolution modeling can lead to notable edge artifacts. One practical solution for reduction of these artifacts, which are also known as Gibbs artifacts, is the use of a kernel width that is smaller than the measured (or true) point spread function.[58] However, these artifacts and the associated variability in the PET counts of small structures are not yet regarded as problems that have been fully resolved.[53]

CT Dose Reduction Techniques

Because of the popular use of hybrid medical imaging systems based on X-ray CT, we should also retain an interest in dose reduction techniques for CT. According to the NCRP report no.

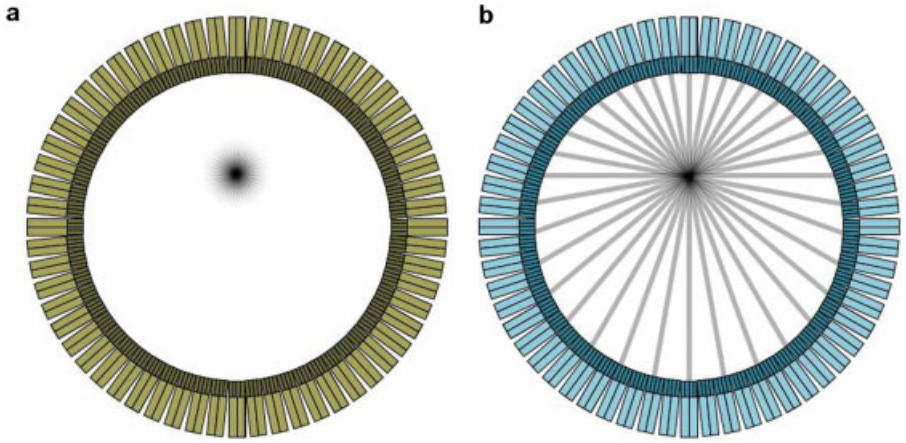

Fig. 12 Noise propagation by back projection in (**a**) time-of-flight (TOF) reconstruction and (**b**) conventional non-TOF reconstruction. (Image courtesy of Dr. Mikiko Ito at GE Healthcare.)

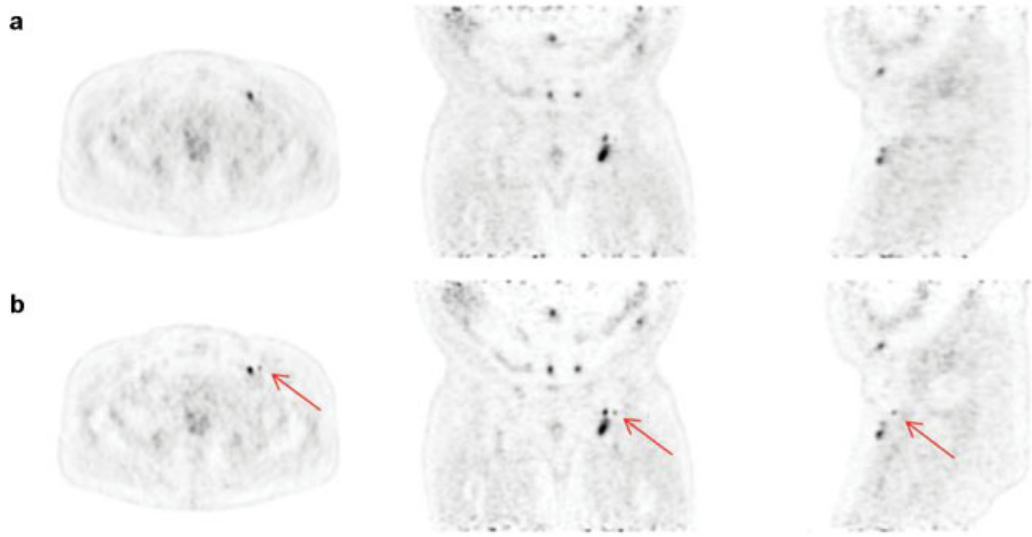

Fig. 13 An example in which the time-of-flight (TOF) PET offers enhanced lesion detectability (arrow) relative to non-TOF PET. (**a**) Non-TOF PET. (**b**) TOF PET. (Reprinted from Conti[52] with permission.)

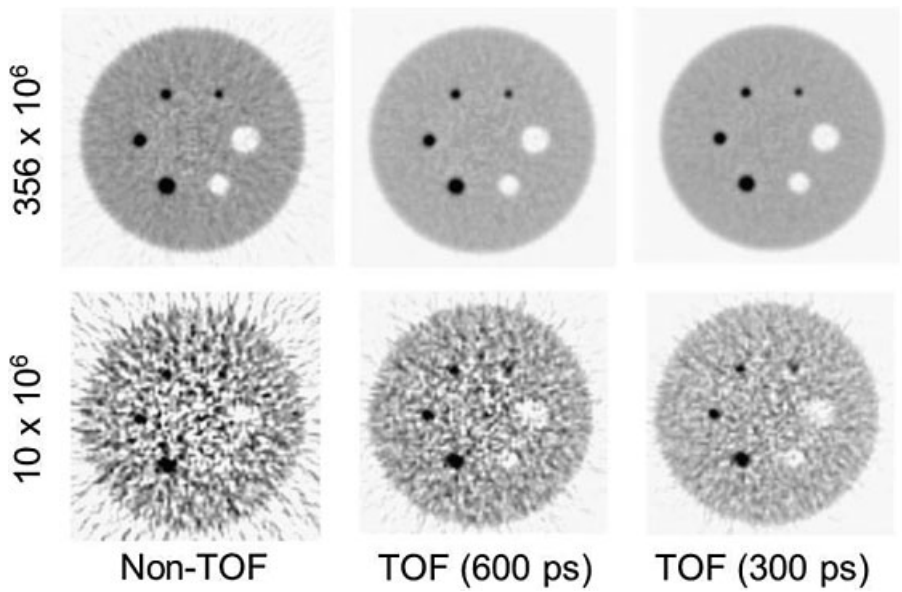

Fig. 14 Monte Carlo simulation of a uniform phantom with high (top) and low (bottom) statistics. Images were reconstructed using the filtered back projection method. TOF, time of flight. (Reprinted from Conti[52] with permission.)

160 of 2009, the level of medical radiation exposure was already comparable with the natural background dose level, and the CT dose was approximately half of the medical radiation exposure level. It is estimated that 67 million CT examinations were performed in the United States alone in 2006, and the applications of CT will continue to grow.[59] Recently, therefore, radiation dose reduction issues have been a topic of discussion for many conferences and communities. Despite the fact that the radiation dose from CT is too small to cause a deterministic effect on the human body, a linear-no-threshold model where the smallest dose is assumed to have the potential to cause a slightly increased cancer risk is usually acceptable.

Radiation dose reduction techniques for CT can generally be categorized into three areas: the hardware system, the reconstruction techniques, and dose control. The radiation dose can be reduced by using better hardware systems. Improved image quality can be achieved through high detection efficiencies and low noise levels. The effectiveness of the detector is determined by both its quantum detection efficiency and its geometrical efficiency. For high quantum detection efficiency, a detector with a rapid response and a short dead time is desirable for the collection of higher numbers of X-ray events.[2] The quantum noise depends on the number of detected events; therefore, a detector with high efficiency can reduce the noise level. Electrical noise,

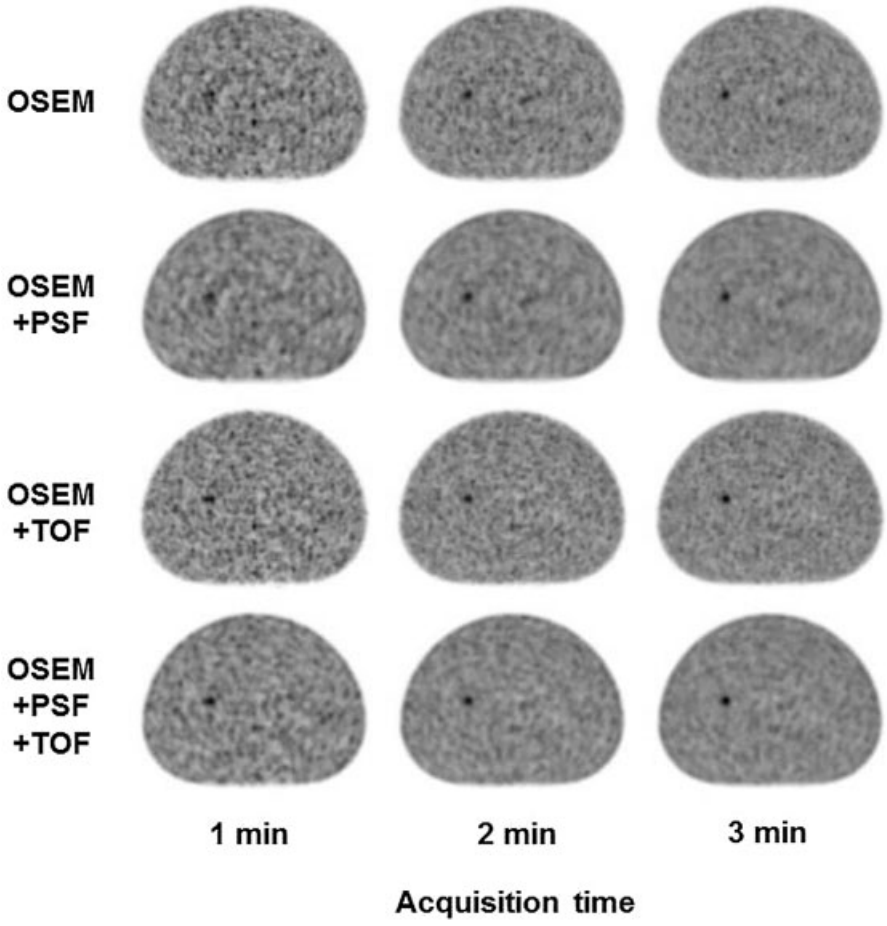

Fig. 15 Image quality enhancement by resolution modeling in PET using point spread function (PSF) and time-of-flight (TOF) information. OSEM, ordered subset expectation maximization. (Reprinted from Akamatsu et al[56] with permission.)

which is caused by fluctuations in the electronic components of the system, is another source of noise, and it should be controlled appropriately. An X-ray beam-sharpening filter offers an important solution for reduction of patient exposure in CT systems. The beam-sharpening filter moderates the X-ray beam to be hard enough to efficiently penetrate the patient while suppressing low-energy X-rays.

Reconstruction techniques are also important tools for reduction of patient radiation exposure. Iterative reconstruction has been widely used in the nuclear medicine field, such

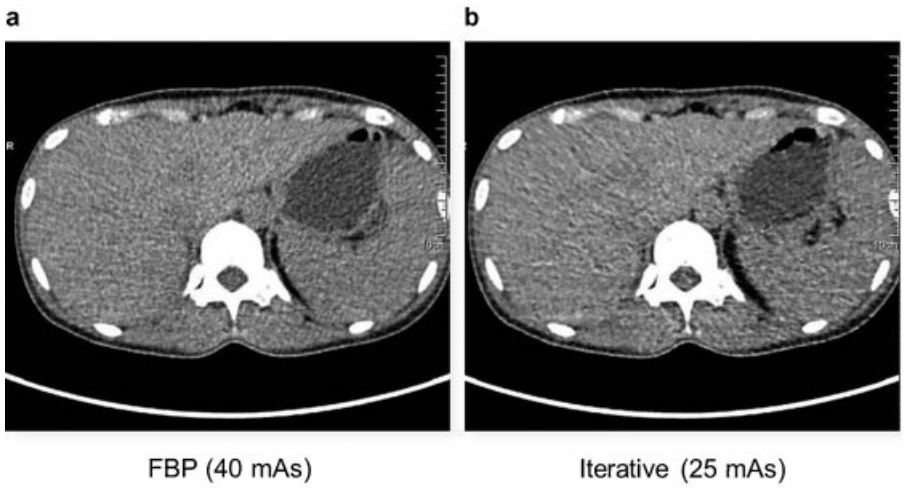

Fig. 16 CT images obtained using (**a**) filtered back projection (FBP) and (**b**) iterative reconstruction. Equivalent image quality relative to the conventional FBP image can be obtained using iterative reconstruction with reduced CT dose.

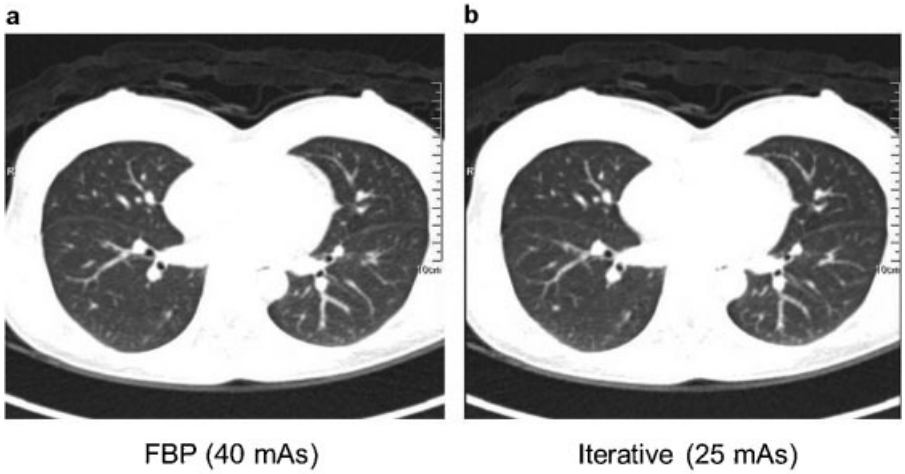

Fig. 17 CT dose reduction by use of iterative reconstruction. CT images obtained using (**a**) filtered back projection (FBP) and (**b**) iterative reconstruction.

as in PET and SPECT systems. Only the FBP was conventionally used for CT because of the heavy computational burden of iterative reconstruction. However, advances in parallel computing have made it possible to apply statistical iterative reconstruction methods to X-ray CT. Compared with conventional FBP CT reconstruction algorithms, iterative reconstruction offers numerous advantages. The use of iterative reconstruction means that lower noise, higher spatial resolution, and reduced image artifacts (e.g., beam hardening and metal artifacts) can be achieved.[3] The system geometry can also be considered for more accurate physical modeling. These properties have the potential to reduce patient dose exposure by reducing the tube current or the CT scan time. Iterative reconstruction can be also incorporated with incomplete data sampling. Compressed sensing was recently introduced as a new reconstruction method for tomographic images, and this method allows accurate image reconstruction from incomplete data sets.[60,61] By using compressed sensing, a reduction of the number of projections is allowed without degradation of the image quality. The major obstacle to iterative reconstruction in CT systems was the heavy computational load; however, computing hardware and software have both improved greatly and the reconstruction time has been significantly shortened.[62–65] As shown in ►**Fig. 16**, the noise reduction provided by iterative reconstruction of CT images is substantial. These CT images show that we can obtain the same image quality with lower tube currents by applying the iterative reconstruction technique. ►**Fig. 17** shows another example of possible CT dose reduction by the use of iterative reconstruction.

The radiation dose exposure can be also reduced by dose control. Photon attenuation is exponentially proportional to an object's thickness; therefore, lower tube currents are sometimes sufficient for lightweight or lean patients. An advanced exposure control method called automatic exposure control (AEC) was also introduced to reduce patient exposure levels.[3,66] Using AEC, the tube current (i.e., the strength of the X-ray beam) can be automatically modulated as a function of the projection angle (angular modulation) and the longitudinal location of the patient's body (z-modulation) using the attenuation information (►**Fig. 18**). Angular modulation is required here because the patient's body shape is not a complete circle. The X-ray exposure level is automatically modulated by the angle based on the direction of the X-ray relative to the patient. For low attenuation areas such as lungs, the tube current is automatically reduced without loss of image quality (z-modulation). The AEC technique is now widely available from the major equipment manufacturers under various trade names.

PET/MR: Newly Emerging Technology

Technical Challenges in PET/MR Systems

As described earlier, in PET scanners, scintillation detectors are used to measure the gamma rays emitted from the

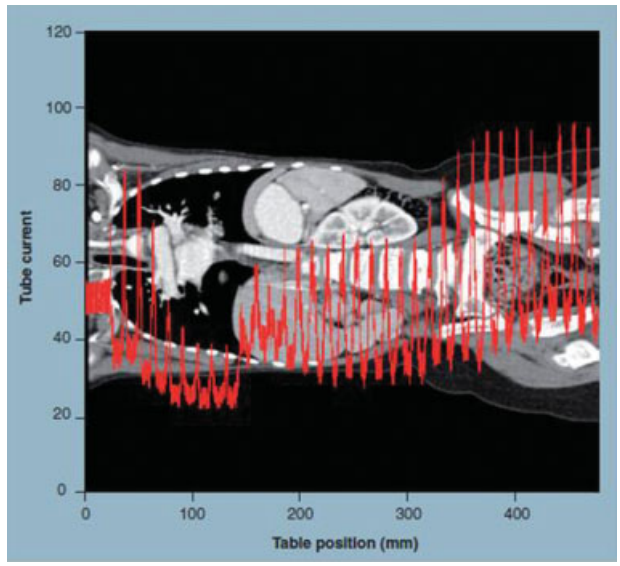

Fig. 18 Automatic exposure control to reduce patient exposure level in X-ray CT. (Reprinted from Yu et al[3] with permission.)

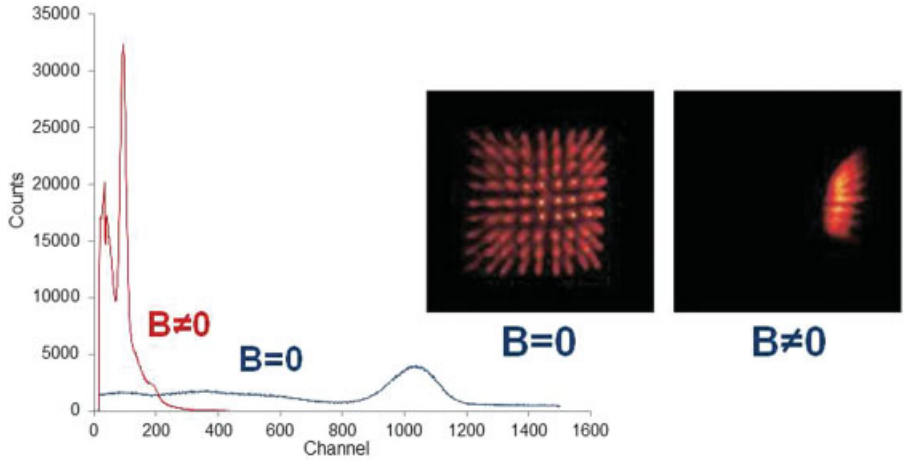

Fig. 19 Distortion of energy spectrum and crystal map of photomultiplier-based scintillation detector. (Reprinted from Lee and Kang[67] and Pichler et al[68] with permission.)

radiopharmaceuticals and consist of arrays of inorganic scintillation crystals and photosensors. Visible or ultraviolet (UV) photons are emitted when the gamma rays are detected by the scintillation crystal and are then measured by the photosensors. The photosensor commonly used in conventional PET (i.e., stand-alone PET or PET/CT) is the photomultiplier tube (PMT), which converts the photons into an electric current that is subsequently amplified by the cascade process of secondary emission. Although PMTs have high signal amplification gain (10^6–10^7) and excellent timing properties, they are highly sensitive to both static and time-varying magnetic fields, which is a major concern in the combination of PET with MRI (►**Fig. 19**).[67,68] The bulky size of PMTs is another reason why the placement of PMT-based PET detectors inside an MR magnet is impractical.

Sequential PET/MR System

A practical solution for combination of a conventional PMT-based PET system with an MR scanner is to transfer patients between two separate machines using a common bed. This approach was adopted in the whole-body PET/MR system produced by Philips Medical Systems (Ingenuity TF PET/MR). In this system, a PMT-based TOF PET is combined with a 3.0-T MRI with a common bed and a common computer console

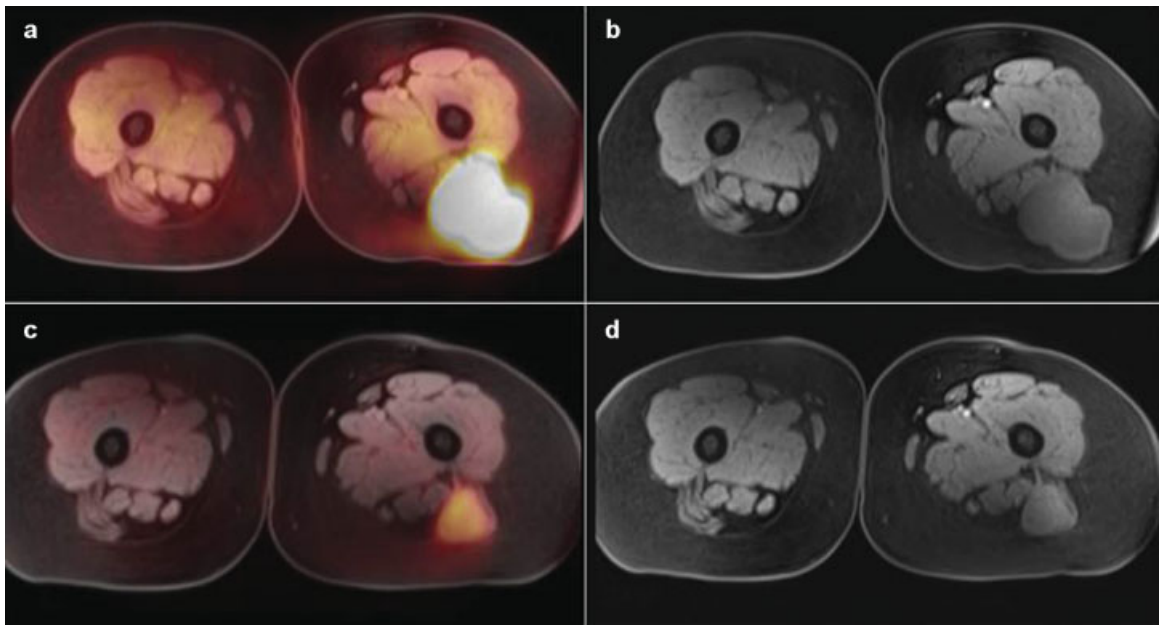

Fig. 20 A 26-year-old female patient who had synovial sarcoma in the left thigh underwent ^{18}F-FDG PET/MR imaging before and after neoadjuvant chemotherapy for staging and to evaluate the treatment efficacy. (**a, b**) On initial PET/MR (DIXON VIBE sequence), images showed lobulated soft tissue tumor in the posterior aspect of left thigh with intense FDG uptake (standard uptake value [SUV]max: 16.3), indicating high-grade synovial sarcoma. (**c, d**) After neoadjuvant chemotherapy, PET/MR and MR image showed decreased size and metabolism of the malignant tumor, reflecting a fair response to the neoadjuvant chemotherapy. However, the remaining mass with moderate hypermetabolism (4.6) suggested the possibility of residual malignant cells, and the result of the postoperative pathologic examination concurred with the imaging finding.

Fig. 21 Photomultiplier-based sequential PET/MR system. (Philips Ingenuity TF PET/MR; image courtesy of Philips Healthcare.)

similar to that of a PET/CT (►**Fig. 21**).[69] Active shielding of the magnetic field from the 3.0-T magnet and additional passive shielding materials around the individual PMTs and the PET gantry allow the two machines to operate in a single room with a distance of ~ 2.5 m between the gantry surfaces. The fronts of the two gantries face each other, and the table is rotated through 180 degrees during the transfer process. This design allows the two systems to be operated under optimal operating conditions with minimal electromagnetic interference. The performance of the PET subsystem was comparable with that of the vendor's stand-alone PET (GEMINI TF PET/CT) when they were compared using both phantom and patient data.[69] The PET subsystem is composed of 28 flat detector modules of 23 × 44 arrays of 4 mm × 4 mm × 22 mm LYSO crystals and has a detector ring diameter of 90.3 cm and an axial field of view (FOV) of 18 cm.[70] A National Electrical Manufacturers Association (NEMA) performance measurement study showed that the transverse and axial resolution near the center was 4.7 mm and the timing and energy resolutions were measured to be 525 ps and 12%, respectively. The absolute sensitivity of the PET scanner was 0.7% (see Zaidi et al[69] for full details of the system specifications and performance). One shortcoming of this design is that the PET and MR data must be acquired sequentially rather than simultaneously.[17] Longer acquisition times because of the sequential acquisition process are the main limitation of this system.

Simultaneous PET/MR System

Simultaneous PET and MR data acquisition using a fully integrated system has several advantages in addition to the shorter scan time when compared with the sequential system. These advantages include the following:

- Temporal correlation of the PET and MR imaging data sets
- Improved spatial correlation because of reduced motion artifacts
- Possible motion correction of the PET data using the MR imaging information

Therefore, several different approaches have been tried to achieve simultaneous PET and MR data acquisition with minimal mutual interference between the PET and MR data. Among these approaches, the feasibility of the use of an avalanche photodiode (APD) rather than a PMT in the PET detector has been demonstrated in prototype preclinical and clinical scanners,[71–73] and a commercial system based on this approach is now available (Biograph mMR from Siemens Healthcare; ►**Fig. 22**). The APD is a semiconductor photosensor that also provides electrical signal amplification through the cascade generation of electron-hole pairs. The APD output signal is only minimally affected by the magnetic field. Another merit of the APD lies in its compact size that allows the integration of the APD-based PET detector with the MR coils. In the Biograph mMR scanner, the APD PET detectors are inserted between the body radiofrequency coil and the gradient coils for simultaneous isocentric data acquisition. The PET system is composed of eight rings of 56 detector blocks that consist of an 8 × 8 array of 4 mm × 4 mm × 20 mm LSO crystals coupled to a 3 × 3 APD array. The system has a transaxial FOV of 59.4 cm and an axial FOV of 25.8 cm. The reduced ring diameter and the longer axial FOV yield a

Fig. 22 Avalanche photodiode–based simultaneous PET/MR system. (Siemens Biograph mMR; image courtesy of Siemens Healthcare.)

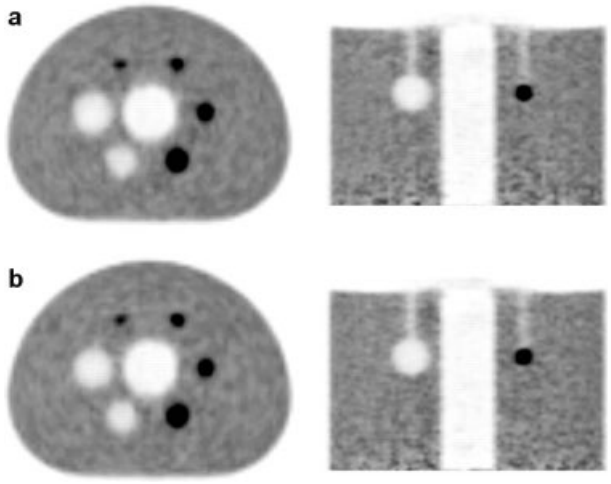

Fig. 23 PET images acquired using avalanche photodiode–based simultaneous PET/MR scanner (**a**) without MR image acquisition and (**b**) with MR image acquisition. (Reprinted from Delso et al[74] with permission.)

high system sensitivity of 1.5% at the center of the PET scanner with an energy window of 430 to 610 keV and a coincidence timing window of 5.86 nanoseconds.[74] This wide coincidence timing window, which causes increased random counts, is used in this scanner because of the poor timing resolution of the APD PET detectors (2.93 nanoseconds), which also disables the TOF measurements (see Ref. [74] for full details of the system specifications and performance). ►**Fig. 23** shows the reconstructed PET images of a body phantom acquired using the Biograph mMR scanner without and with MR image acquisition, demonstrating no artifacts due to the simultaneous data acquisition.

Next-Generation PET/MR Systems

The silicon photomultiplier (SiPM) is regarded as an alternative to APD photosensors for the next generation of PET/MR scanners because the SiPM has much higher internal gain ($\sim 10^6$) and faster timing properties than the APD.[75,76] The SiPM is composed of an array of APD cells operating in Geiger mode; each cell, when struck by a photon, generates an avalanche of electrons. The SiPM is also compact and insensitive to magnetic fields, similar to conventional APDs.[75,77] The feasibility of SiPM-based PET detectors and systems has been demonstrated by several groups for applications including small animal imaging,[78,79] depth-of-interaction measurements,[80,81] and simultaneous PET/MR imaging (►**Fig. 24** and ►**Fig. 25**).[82] Additionally, the high gain and fast response of the SiPM enables TOF PET detection in clinical PET/MR scanners with excellent timing resolution. In the prototype PET/MR system that is under development by GE Healthcare, the SiPM-based TOF PET scanner has been combined with a 3.0-T MR scanner and yields timing resolution of $\sim$ 390 ps (►**Fig. 26**).[83] The SiPM PET system features five rings of 112 detector blocks (each of which is a 4×9 array of LYSO crystals, 3.95 mm $\times$ 5.3 mm $\times$ 25 mm in size) coupled to 1×3 arrays of SiPM devices, with a transaxial FOV of 60 cm and an axial FOV of 25 cm.[83]

Attenuation Correction: Unsolved Issue in PET/MR

As described earlier, PET scanners detect annihilation photons (gamma rays) emitted from positron-electron interactions. These gamma rays then interact with matter as they pass through the body. The interaction of the photons with matter through photoelectric absorption and Compton scattering processes result in photon attenuation. For accurate quantification of the radiopharmaceutical density (kBq/ml or μCi/cc), the photon attenuation should therefore be corrected appropriately. ►**Fig. 27** shows the effects of photon attenuation in emission PET images. The radiopharmaceutical density is severely underestimated at the center of the object (or the patient) in the PET image without the appropriate attenuation correction. Inaccurate attenuation correction leads to quantification errors and/or the misinterpretation of lesions. Therefore, attenuation correction is a mandatory process in emission PET scans.

In PET/CT systems, the attenuation correction process is performed by use of the CT images. Because the X-ray photon attenuation is mainly determined by the electron density of the material, the CT pixel value that is usually presented as the Hounsfield unit reflects the photon attenuation properties. The relationship between the CT Hounsfield unit and the attenuation coefficient for 511-keV gamma-ray photons has been investigated by several research groups.[84–86] The

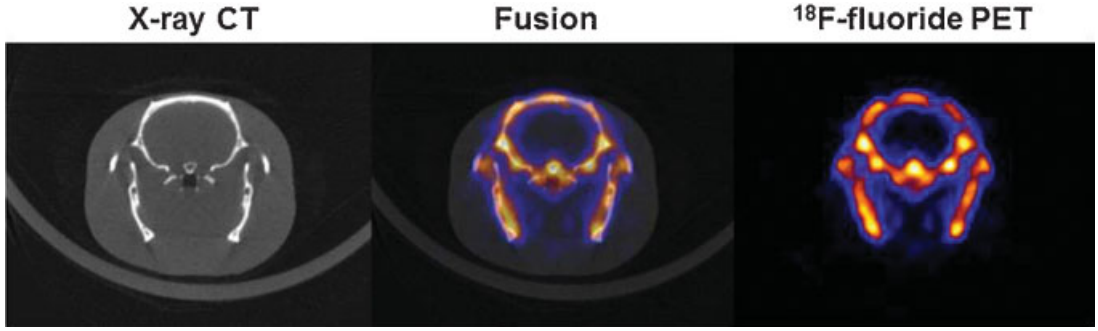

Fig. 24 ^{18}F-fluoride PET images of rat skull acquired using a silicon photomultiplier–based small animal PET (Reprinted from Kwon et al[79] with permission.)

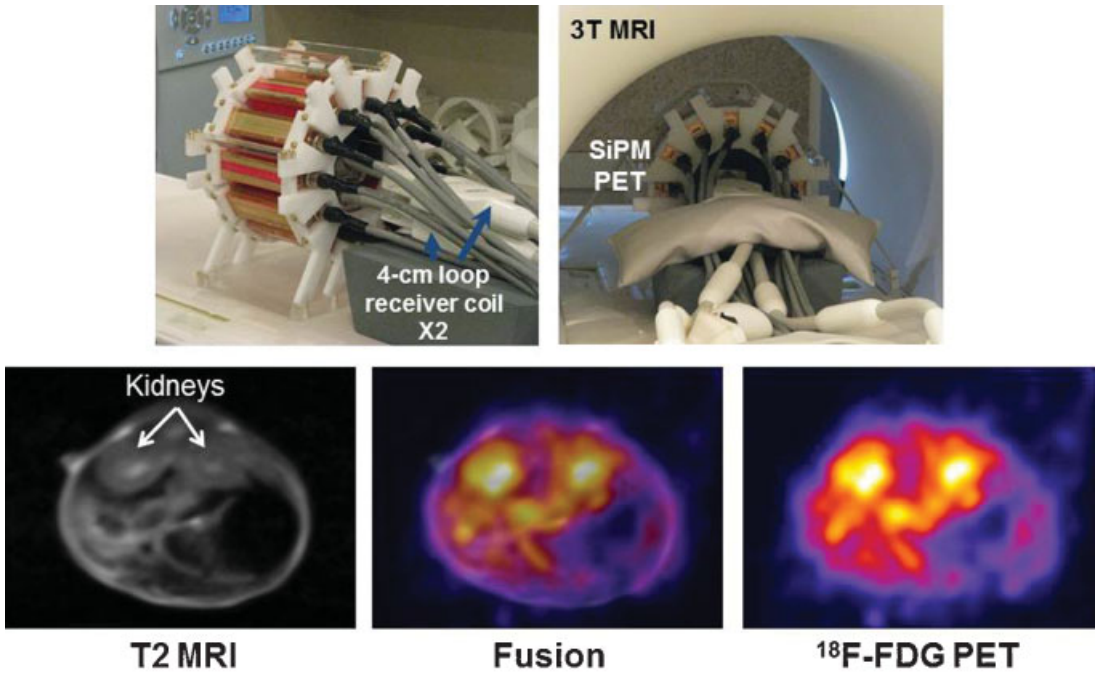

Fig. 25 Simultaneous PET/MR image acquisition using MR-compatible silicon photomultiplier–based small animal PET. (Reprinted from Yoon et al[82] with permission.)

bilinear transformation shown in ►**Fig. 28** is currently used as a simple solution to obtain the attenuation coefficient map of a 511-keV gamma ray from the Hounsfield unit in the CT image. Attenuation correction factors for each LOR are then generated based on the line integral of the attenuation coefficient map along the LOR.

In PET/MR systems, CT images are not available. The MR images reflect the proton densities or the relaxation properties; therefore, the MR intensity itself is not proportional to the photon attenuation power.[87] In CT images, pixels with high intensity can be matched with highly attenuating materials, but this relationship cannot be applied in MR images. For example, in MRI, the bone structures in the body with the highest densities usually show low pixel values and cannot be distinguished from the air.

Several approaches have been suggested for PET attenuation correction in PET/MR systems; these methods can be categorized into template-guided and segmentation-based attenuation correction approaches. The template-guided attenuation correction method uses the template images of the attenuation map and a spatial normalization algorithm to transform the template into an individual attenuation map.[88–90] However, the use of the relatively robust template-guided attenuation correction is possible only for the brain because current spatial normalization methods cannot fully accommodate the wide interindividual anatomical

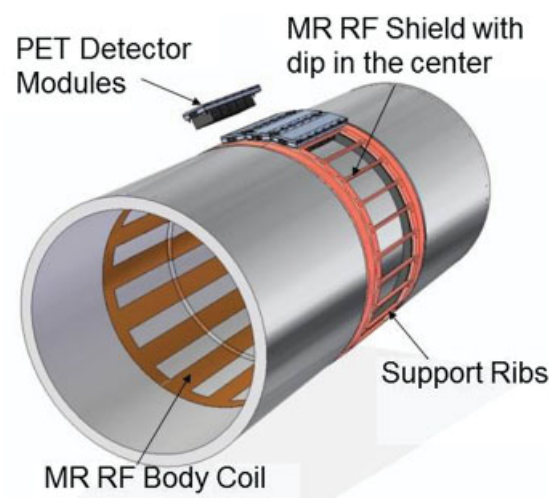

Fig. 26 Silicon photomultiplier–based time-of-flight PET scanner combined with a 3.0-T MR scanner. RF, radiofrequency. (Image courtesy of GE Healthcare.)

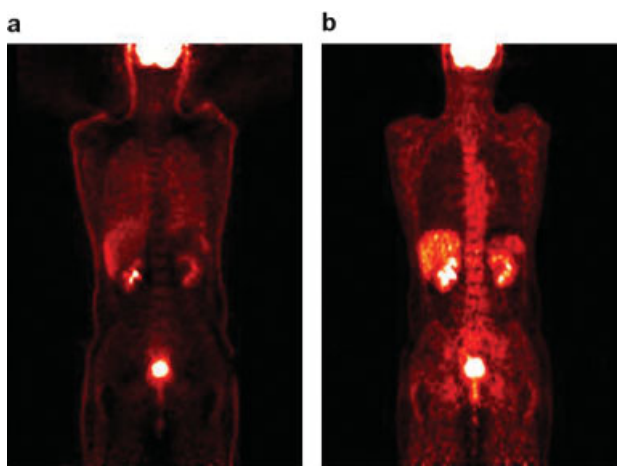

Fig. 27 Whole-body PET images (**a**) without attenuation correction and (**b**) after attenuation correction.

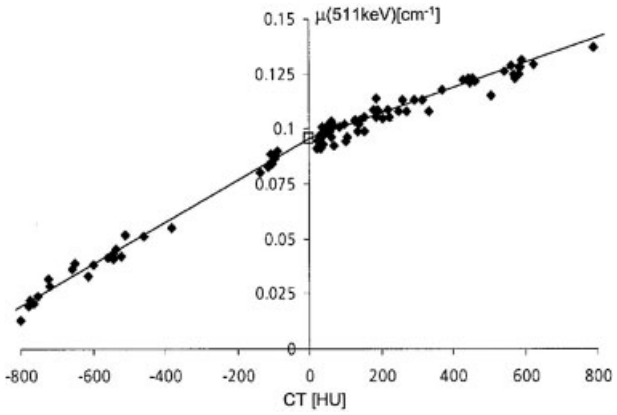

Fig. 28 Bilinear transformation currently used to obtain the attenuation coefficient map of a 511-keV gamma ray from the Hounsfield unit (HU) in the CT image. (Reprinted from Burger et al[84] with permission.)

variability of whole-body images. The segmentation-based attenuation correction method segments and categorizes tissue groups on the basis of their MR intensities.[91,92] Representative attenuation coefficient values are assigned to each segmented tissue group. In current commercial PET/MR systems, a two-point Dixon MRI sequence is used for the segmentation-based attenuation correction process in which an attenuation map comprising four segments (water-equivalent tissue, fat, lung, and air in the body) is provided (►**Fig. 29**).[92] However, bone segmentation in whole-body images has not been successful because it is difficult to distinguish between the bone and air intensities in MR images that were acquired using standard MR sequences.[93] The relaxation time of protons in bone structures is too short to measure the signal intensities, and as a result, bone and air show similar intensity levels.

An approach for measurement of the early bone signals using the ultrashort echo time (UTE) MR sequences before they rapidly disappear is used for bone segmentation in PET/MR (►**Fig. 30**).[94–96] However, the boundary regions between soft tissues and air are sometimes misinterpreted as bone structures, which leads to large errors in the reconstructed PET images.[96] Consequently, the UTE sequence is limited to use for segmentation of the bone structures in the head, which is a relatively simple structure.

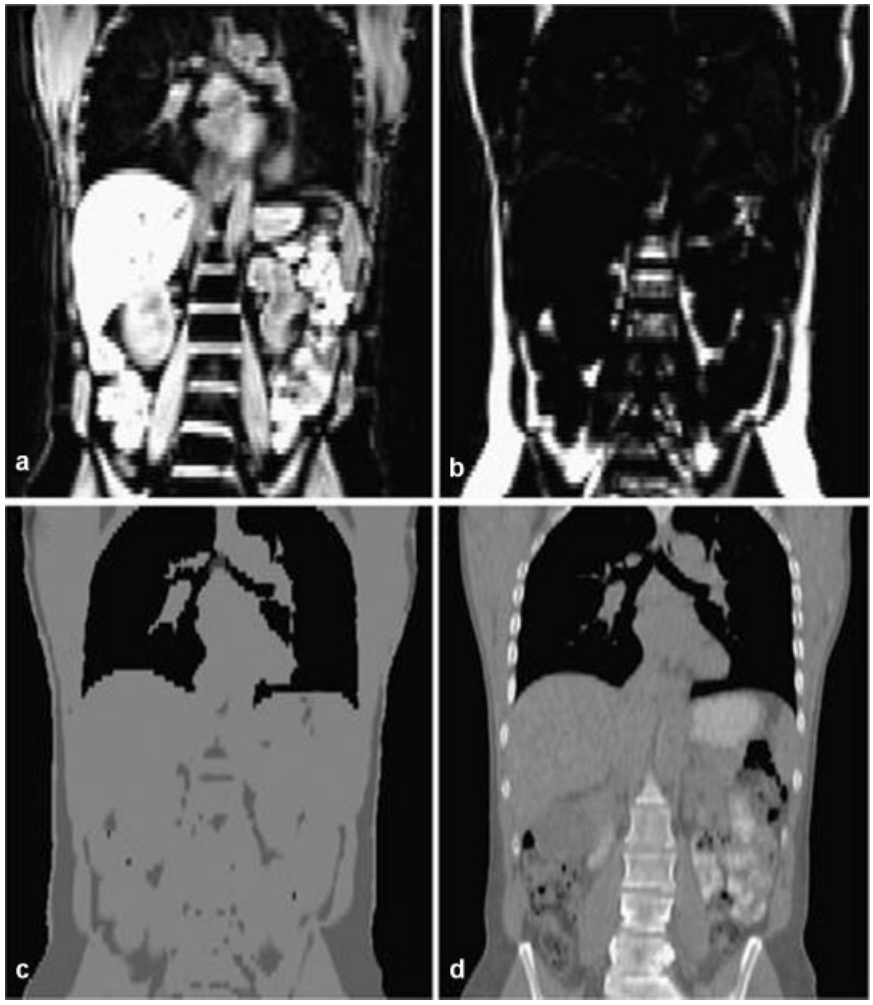

Fig. 29 Generation of PET attenuation map using two-point Dixon MRI sequence. (**a**) MR water image. (**b**) Fat image. (**c**) MR-based attenuation map produced by combining water and fat images. (**d**) CT-based attenuation map of same patient. (Reprinted from Martinez-Möller et al[92] with permission.)

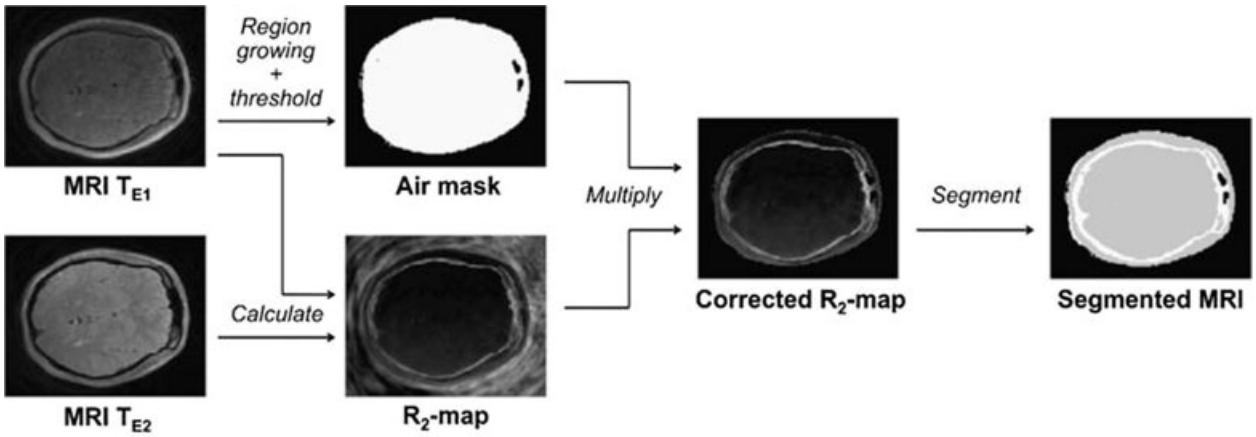

Fig. 30 Generation of PET attenuation map using ultrashort echo time MR sequence. MR images acquired at two different echo times (T_{E1} and T_{E2}) are used to create R_2 map and MR-based attenuation map. (Reprinted from Catana et al[96] with permission.)

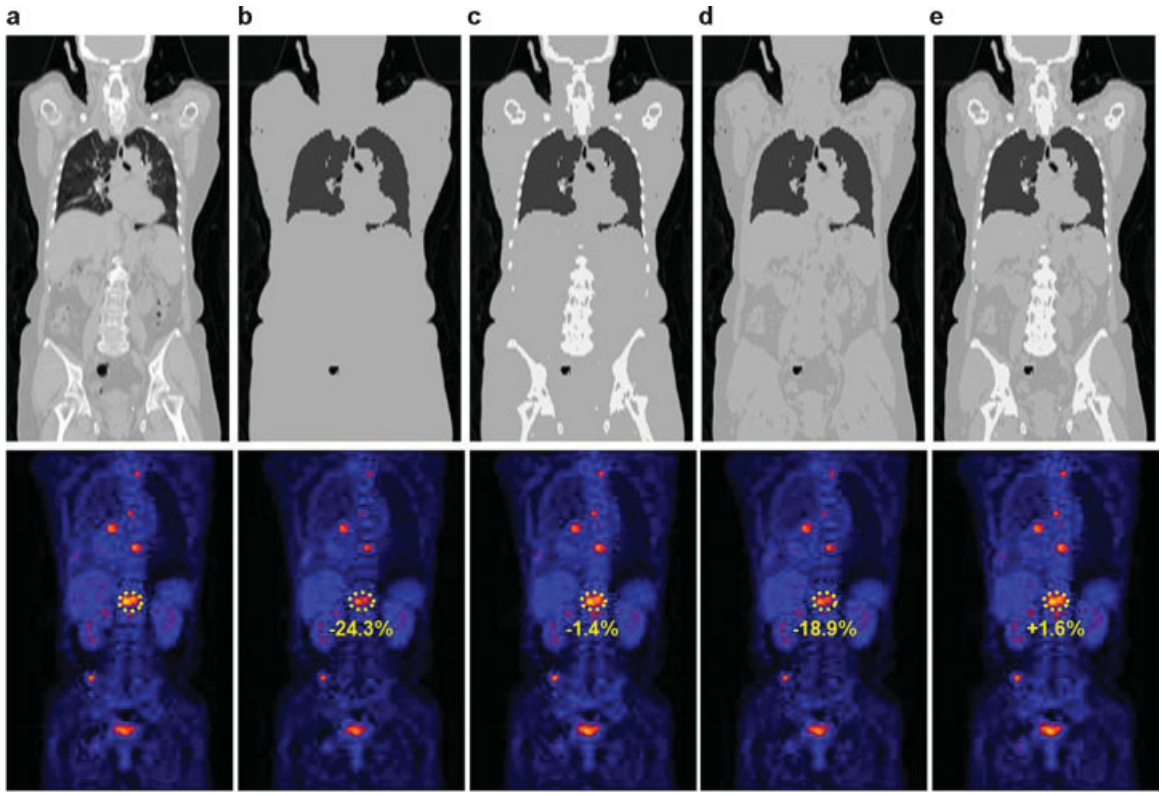

Fig. 31 Attenuation coefficient maps (top) and PET images corrected using them (bottom). (**a**) Original CT image and attenuation coefficient maps with different approaches. (**b**) Soft tissue/lung/air segmentation. (**c**) Soft tissue/lungs/air/bone. (**d**) Water/fat/lung/air. (**e**) Water/fat/lung/air/bone. The values written below the marked lesion are the percentage differences of standard uptake value relative to CT-based attenuation correction. (Reprinted from Kim et al[97] with permission.)

The effects of the attenuation correction of PET images without bone segmentation in whole-body images were evaluated by several groups.[97,98] These studies all showed that PET attenuation correction without consideration of the bone attenuation resulted in highly inaccurate PET quantification in both bones and the surrounding tissues (14.7–16.4% negative bias in the spinal bones,[97] and 12.4% for malignant bone lesions and 30.1% for normal bone[98]) (►**Fig. 31**). It should be also noted that variations in the tissue density within organs or segments also can lead to PET quantification errors.[97,99] Further developments to improve the attenuation correction processes in PET/MR systems are required.

Conclusion

Modern hybrid medical imaging systems and recent advances in the hardware and software techniques used in those systems were reviewed briefly in this article. Advanced

detection materials, detection electronics, and processing and reconstruction algorithms offer hybrid imaging systems with rapid scan times and low patient radiation exposure. Complementary anatomical, functional, and molecular information measured in the convenient one-stop examinations provided by the PET/CT and SPECT/CT systems have made these modalities into primary diagnostic tools in many cases. Although the system is in an early stage of adaptation, with some limitations in terms of quantitative accuracy and a continuing debate with regard to its ultimate role, the PET/MR system is regarded as another major breakthrough in modern biomedical engineering with great potential for widespread use in clinical practice.

Acknowledgments

The authors express gratitude to Hyung Jun Im, nuclear medicine physician, and Yong Ho Do and Hyeong Jin Lee, nuclear medicine technologists, at Seoul National University Hospital, Seoul, Korea, for providing most of clinical images presented in this article. This work was supported by grants 10030030, HI13C-0163–020013, and 2013013175 from the Ministry of Trade, Industry and Energy, the Ministry of Health and Welfare, and the NRF funded by the Ministry of Science, ICT, and Future Planning.

References

1 Rybicki FJ, Otero HJ, Steigner ML, et al. Initial evaluation of coronary images from 320-detector row computed tomography. Int J Cardiovasc Imaging 2008;24(5):535–546
2 Hsieh J. Computed Tomography: Principles, Design, Artifacts, and Recent Advances. 2nd ed. Bellingham, WA: SPIE; 2009
3 Yu L, Liu X, Leng S, et al. Radiation dose reduction in computed tomography: techniques and future perspective. Imaging Med 2009;1(1):65–84
4 Blamire AM. The technology of MRI—the next 10 years? Br J Radiol 2008;81(968):601–617
5 Gold GE, Chen CA, Koo S, Hargreaves BA, Bangerter NK. Recent advances in MRI of articular cartilage. AJR Am J Roentgenol 2009; 193(3):628–638
6 Kim K-N, Jeong H, Heo P, et al. Improving RF field strength and uniformity in a local region by controlling individual transmitting RF phase in a 7T tranceive array coil. Biomed Eng Lett 2012;2(4): 223–232
7 Pomper MG, Lee JS. Small animal imaging in drug development. Curr Pharm Des 2005;11(25):3247–3272
8 Hill DLG, Batchelor PG, Holden M, Hawkes DJ. Medical image registration. Phys Med Biol 2001;46(3):R1–R45
9 Zitová B, Flusser J. Image registration methods: a survey. Image Vis Comput 2003;21:977–1000
10 Lee JS, Park KS, Lee DS, Lee CW, Chung JK, Lee MC. Development and applications of a software for Functional Image Registration (FIRE). Comput Methods Programs Biomed 2005;78(2):157–164
11 Gaidhane VH, Hote YV, Singh V. Nonrigid image registration using efficient similarity measure and Levenberg-Marquardt optimization. Biomed Eng Lett 2012;2(2):118–123
12 LaCroix KJ, Tsui BMW, Hasegawa BH, Brown JK. Investigation of the use of x-ray CT images for attenuation correction in SPECT. IEEE Trans Nucl Sci 1994;41:2793–2799
13 Blankespoor SC, Xu X, Kaiki K, et al. Attenuation correction of SPECT using X-ray CT on an emission-transmission CT system: myocardial perfusion assessment. IEEE Trans Nucl Sci 1996;43(4): 2263–2274
14 Seo Y, Mari C, Hasegawa BH. Technological development and advances in single-photon emission computed tomography/computed tomography. Semin Nucl Med 2008;38(3):177–198
15 Beyer T, Townsend DW, Brun T, et al. A combined PET/CT scanner for clinical oncology. J Nucl Med 2000;41(8):1369–1379
16 Townsend DW. Dual-modality imaging: combining anatomy and function. J Nucl Med 2008;49(6):938–955
17 Zaidi H, Alavi A. Current trends in PET and combined (PET/CT and PET/MR) systems design. PET Clin 2007;2(2):109–123
18 Lee JS. Technical advances in current PET and hybrid imaging systems. Open Nucl Med J 2010;2:192–208
19 Shao Y, Cherry SR, Farahani K, et al. Simultaneous PET and MR imaging. Phys Med Biol 1997;42(10):1965–1970
20 Raylman RR, Majewski S, Lemieux SK, et al. Simultaneous MRI and PET imaging of a rat brain. Phys Med Biol 2006;51(24):6371–6379
21 Cherry SR. Multimodality imaging: beyond PET/CT and SPECT/CT. Semin Nucl Med 2009;39(5):348–353
22 Hicks RJ, Hofman MS. Is there still a role for SPECT-CT in oncology in the PET-CT era? Nat Rev Clin Oncol 2012;9(12):712–720
23 Saha S, Burke C, Desai A, Vijayanathan S, Gnanasegaran G. SPECT-CT: applications in musculoskeletal radiology. Br J Radiol 2013; 86(1031):20120519
24 Hung NM, Joung J, Lee K, Kim Y. Development of correction schemes for a small field of view gamma camera. Biomed Eng Lett 2012;2(4):215–222
25 Cherry SR, Sorenson JA, Phelps ME. Physics in Nuclear Medicine. 4th ed. Philadelphia, PA: Elsevier Saunders; 2012
26 Anger HO. Scintillation camera. Rev Sci Instrum 1957;29:27–33
27 Anger HO. Scintillation camera with multichannel collimators. J Nucl Med 1964;5:515–531
28 Zeng GL, Galt JR, Wernick MN, Mintzer RA, Aarsvold JN. Single-photon emission computed tomography. In: Wernick MN, Aarsvold JN, eds. Emission Tomography: The Fundamentals of PET and SPECT. San Diego, CA: Elsevier; 2004:127–152
29 Peterson TE, Furenlid LR. SPECT detectors: the Anger Camera and beyond. Phys Med Biol 2011;56(17):R145–R182
30 CZT technology: fundamentals and applications. GE Heathcare White Paper 2010. Available at:http://www3.gehealthcare.com/~/media/Downloads/us/Product/Categories/Nuclear-Medicine/Cardiac%20Scanners/Discovery-NM570c/GEHealthcare-Whitepaper_CZT-Technology-20111201.pdf. Accessed on March 18, 2014
31 Patton JA, Slomka PJ, Germano G, Berman DS. Recent technologic advances in nuclear cardiology. J Nucl Cardiol 2007;14(4):501–513
32 Erlandsson K, Kacperski K, van Gramberg D, Hutton BF. Performance evaluation of D-SPECT: a novel SPECT system for nuclear cardiology. Phys Med Biol 2009;54(9):2635–2649
33 Esteves FP, Raggi P, Folks RD, et al. Novel solid-state-detector dedicated cardiac camera for fast myocardial perfusion imaging: multicenter comparison with standard dual detector cameras. J Nucl Cardiol 2009;16(6):927–934
34 DePuey EG. Advances in SPECT camera software and hardware: currently available and new on the horizon. J Nucl Cardiol 2012; 19(3):551–581; quiz 585
35 Garcia EV, Faber TL, Esteves FP. Cardiac dedicated ultrafast SPECT cameras: new designs and clinical implications. J Nucl Med 2011; 52(2):210–217
36 Frey E, Tsui B. Collimator-detector response compensation in SPECT. In: Zaidi H, ed. Quantitative Analysis of Nuclear Medicine Images. New York, NY: Springer; 2006:141–166
37 Rahmim A, Zaidi H. PET versus SPECT: strengths, limitations and challenges. Nucl Med Commun 2008;29(3):193–207
38 Ritt P, Vija H, Hornegger J, Kuwert T. Absolute quantification in SPECT. Eur J Nucl Med Mol Imaging 2011;38(Suppl 1):S69–S77

39 Stansfield EC, Sheehy N, Zurakowski D, Vija AH, Fahey FH, Treves ST. Pediatric 99mTc-MDP bone SPECT with ordered subset expectation maximization iterative reconstruction with isotropic 3D resolution recovery. Radiology 2010;257(3):793–801

40 Bailey DL, Willowson KP. An evidence-based review of quantitative SPECT imaging and potential clinical applications. J Nucl Med 2013;54(1):83–89

41 Bailey DL. Transmission scanning in emission tomography. Eur J Nucl Med 1998;25(7):774–787

42 Zaidi H, Hasegawa B. Determination of the attenuation map in emission tomography. J Nucl Med 2003;44(2):291–315

43 Vija H. Introduction to xSPECT technology: evolving multi-modal SPECT to become context-based and quantitative. Siemens Medical Solutions USA Inc. White Paper 2013. Available at:http://www.healthcare.siemens.com/siemens_hwem-hwen_ssxa_websites-context-root/wcm/idc/groups/public/@global/@imaging/@molecular/documents/download/mdax/ote3/~edisp/xspect_technical_white_paper-00957532.pdf. Accessed on: March 18, 2014

44 Costelloe CM, Murphy WA Jr, Chasen BA. Musculoskeletal pitfalls in 18F-FDG PET/CT: pictorial review. AJR Am J Roentgenol 2009; 193(3, Suppl):WS1–WS13; quiz S26–S30

45 Lakkaraju A, Patel CN, Bradley KM, Scarsbrook AF. PET/CT in primary musculoskeletal tumours: a step forward. Eur Radiol 2010;20(12):2959–2972

46 Fischer DR. Musculoskeletal imaging using fluoride PET. Semin Nucl Med 2013;43(6):427–433

47 Yoon SH, Kim KS, Kang SY, et al. Usefulness of 18F-fluoride PET/CT in breast cancer patients with osteosclerotic bone metastases. Nucl Med Mol Imaging 2013;47(1):27–35

48 Grant FD, Fahey FH, Packard AB, Davis RT, Alavi A, Treves ST. Skeletal PET with 18F-fluoride: applying new technology to an old tracer. J Nucl Med 2008;49(1):68–78

49 Kang JY, Lee WW, So Y, Lee BC, Kim SE. Clinical usefulness of ^{18}F-fluoride bone PET. Nucl Med Mol Imaging 2010;44(1):55–61

50 Lewellen TK. Recent developments in PET detector technology. Phys Med Biol 2008;53(17):R287–R317

51 Ito M, Hong SJ, Lee JS. Positron emission tomography (PET) detectors with depth-of-interaction (DOI) capability. Biomed Eng Lett 2011;1(2):70–81

52 Conti M. Focus on time-of-flight PET: the benefits of improved time resolution. Eur J Nucl Med Mol Imaging 2011;38(6):1147–1157

53 Rahmim A, Qi J, Sossi V. Resolution modeling in PET imaging: theory, practice, benefits, and pitfalls. Med Phys 2013;40(6):064301

54 Alessio AM, Kinahan PE, Lewellen TK. Modeling and incorporation of system response functions in 3D whole body PET. IEEE Nucl Sci Symp Conf Rec 2004;6:3992–3996

55 Kadrmas DJ, Casey ME, Conti M, Jakoby BW, Lois C, Townsend DW. Impact of time-of-flight on PET tumor detection. J Nucl Med 2009; 50(8):1315–1323

56 Akamatsu G, Ishikawa K, Mitsumoto K, et al. Improvement in PET/CT image quality with a combination of point-spread function and time-of-flight in relation to reconstruction parameters. J Nucl Med 2012;53(11):1716–1722

57 Schaefferkoetter J, Casey M, Townsend D, El Fakhri G. Clinical impact of time-of-flight and point response modeling in PET reconstructions: a lesion detection study. Phys Med Biol 2013; 58(5):1465–1478

58 Watson CC. Estimating effective model kernel widths for PSF reconstruction in PET. IEEE Nucl Sci Symp Conf Rec 2011: 2368–2374

59 National Council on Radiation Protection & Measurements (NCRP). Report no. 160: Ionizing radiation exposure of the population of the United States (2009). Available at: http://www.ncrppublications.org/Reports/160. Accessed January 9, 2014

60 Chen GH, Tang J, Leng S. Prior image constrained compressed sensing (PICCS): a method to accurately reconstruct dynamic CT images from highly undersampled projection data sets. Med Phys 2008;35(2):660–663

61 Sidky EY, Pan X. Image reconstruction in circular cone-beam computed tomography by constrained, total-variation minimization. Phys Med Biol 2008;53(17):4777–4807

62 Beekma FJ, Kamphuis C. Ordered subset reconstruction for x-ray CT. Phys Med Biol 2001;46(7):1835–1844

63 Kole JS, Beekman FJ. Evaluation of accelerated iterative x-ray CT image reconstruction using floating point graphics hardware. Phys Med Biol 2006;51(4):875–889

64 Sharp GC, Kandasamy N, Singh H, Folkert M. GPU-based streaming architectures for fast cone-beam CT image reconstruction and demons deformable registration. Phys Med Biol 2007;52(19): 5771–5783

65 Silva AC, Lawder HJ, Hara A, Kujak J, Pavlicek W. Innovations in CT dose reduction strategy: application of the adaptive statistical iterative reconstruction algorithm. AJR Am J Roentgenol 2010; 194(1):191–199

66 McCollough CH, Bruesewitz MR, Kofler JM Jr. CT dose reduction and dose management tools: overview of available options. Radiographics 2006;26(2):503–512

67 Lee JS, Kang KW. PET/MRI. In: Kim EE, Lee MC, Inoue T, Wong W-H, eds. Clinical PET and PET/CT: Principles and Applications. New York, NY: Springer; 2013:373–390

68 Pichler BJ, Wehrl HF, Kolb A, Judenhofer MS. Positron emission tomography/magnetic resonance imaging: the next generation of multimodality imaging? Semin Nucl Med 2008;38(3):199–208

69 Zaidi H, Ojha N, Morich M, et al. Design and performance evaluation of a whole-body Ingenuity TF PET-MRI system. Phys Med Biol 2011;56(10):3091–3106

70 Surti S, Kuhn A, Werner ME, Perkins AE, Kolthammer J, Karp JS. Performance of Philips Gemini TF PET/CT scanner with special consideration for its time-of-flight imaging capabilities. J Nucl Med 2007;48(3):471–480

71 Catana C, Wu Y, Judenhofer MS, Qi J, Pichler BJ, Cherry SR. Simultaneous acquisition of multislice PET and MR images: initial results with a MR-compatible PET scanner. J Nucl Med 2006; 47(12):1968–1976

72 Pichler BJ, Judenhofer MS, Catana C, et al. Performance test of an LSO-APD detector in a 7-T MRI scanner for simultaneous PET/MRI. J Nucl Med 2006;47(4):639–647

73 Schlemmer HP, Pichler BJ, Schmand M, et al. Simultaneous MR/PET imaging of the human brain: feasibility study. Radiology 2008; 248(3):1028–1035

74 Delso G, Fürst S, Jakoby B, et al. Performance measurements of the Siemens mMR integrated whole-body PET/MR scanner. J Nucl Med 2011;52(12):1914–1922

75 Lee JS, Hong SJ. Geiger-mode avalanche photodiodes for PET/MRI. In: Iniewski K, ed. Electronic Circuits for Radiation Detection. Boca Raton, FL: CRC Press; 2010:179–200

76 Roncali E, Cherry SR. Application of silicon photomultipliers to positron emission tomography. Ann Biomed Eng 2011;39(4): 1358–1377

77 Hong SJ, Song IC, Ito M, et al. An investigation into the use of Geiger-mode solid-state photomultipliers for simultaneous PET and MRI acquisition. IEEE Trans Nucl Sci 2008;55(3):882–888

78 Yamamoto S, Imaizumi M, Watabe T, et al. Development of a Si-PM-based high-resolution PET system for small animals. Phys Med Biol 2010;55(19):5817–5831

79 Kwon SI, Lee JS, Yoon HS, et al. Development of small-animal PET prototype using silicon photomultiplier (SiPM): initial results of phantom and animal imaging studies. J Nucl Med 2011;52(4): 572–579

80 Yamaya T, Mitsuhashi T, Matsumoto T, et al. A SiPM-based isotropic-3D PET detector X'tal cube with a three-dimensional array of 1 mm(3) crystals. Phys Med Biol 2011;56(21):6793–6807

81 Ko GB, Yoon HS, Kwon SI, et al. Development of a front-end analog circuit for multi-channel SiPM readout and performance verification for various PET detector designs. Nucl Instr Meth A 2013; 703:38–44

82 Yoon HS, Ko GB, Kwon SI, et al. Initial results of simultaneous PET/MRI experiments with an MRI-compatible silicon photomultiplier PET scanner. J Nucl Med 2012;53(4):608–614
83 Levin C, Glover G, Deller T, McDaniel D, Peterson W, Maramraju SH. Prototype time-of-flight PET ring integrated with a 3T MRI system for simultaneous whole-body PET/MR imaging. J Nucl Med 2013; 54(Suppl 2):148
84 Burger C, Goerres G, Schoenes S, Buck A, Lonn AH, Von Schulthess GK. PET attenuation coefficients from CT images: experimental evaluation of the transformation of CT into PET 511-keV attenuation coefficients. Eur J Nucl Med Mol Imaging 2002;29(7):922–927
85 Kinahan PE, Hasegawa BH, Beyer T. X-ray-based attenuation correction for positron emission tomography/computed tomography scanners. Semin Nucl Med 2003;33(3):166–179
86 Carney JP, Townsend DW, Rappoport V, Bendriem B. Method for transforming CT images for attenuation correction in PET/CT imaging. Med Phys 2006;33(4):976–983
87 Hofmann M, Steinke F, Scheel V, et al. MRI-based attenuation correction for PET/MRI: a novel approach combining pattern recognition and atlas registration. J Nucl Med 2008;49(11):1875–1883
88 Schreibmann E, Nye JA, Schuster DM, Martin DR, Votaw J, Fox T. MR-based attenuation correction for hybrid PET-MR brain imaging systems using deformable image registration. Med Phys 2010; 37(5):2101–2109
89 Kim JS, Lee JS, Park MH, et al. Feasibility of template-guided attenuation correction in cat brain PET imaging. Mol Imaging Biol 2010;12(3):250–258
90 Malone IB, Ansorge RE, Williams GB, Nestor PJ, Carpenter TA, Fryer TD. Attenuation correction methods suitable for brain imaging with a PET/MRI scanner: a comparison of tissue atlas and template attenuation map approaches. J Nucl Med 2011;52(7):1142–1149
91 Schulz V, Torres-Espallardo I, Renisch S, et al. Automatic, three-segment, MR-based attenuation correction for whole-body PET/MR data. Eur J Nucl Med Mol Imaging 2011;38(1):138–152
92 Martinez-Möller A, Souvatzoglou M, Delso G, et al. Tissue classification as a potential approach for attenuation correction in whole-body PET/MRI: evaluation with PET/CT data. J Nucl Med 2009; 50(4):520–526
93 Hofmann M, Pichler B, Schölkopf B, Beyer T. Towards quantitative PET/MRI: a review of MR-based attenuation correction techniques. Eur J Nucl Med Mol Imaging 2009;36(Suppl 1):S93–S104
94 Johansson A, Karlsson M, Nyholm T. CT substitute derived from MRI sequences with ultrashort echo time. Med Phys 2011;38(5): 2708–2714
95 Catana C, van der Kouwe A, Benner T, et al. Toward implementing an MRI-based PET attenuation-correction method for neurologic studies on the MR-PET brain prototype. J Nucl Med 2010;51(9): 1431–1438
96 Keereman V, Fierens Y, Broux T, De Deene Y, Lonneux M, Vandenberghe S. MRI-based attenuation correction for PET/MRI using ultrashort echo time sequences. J Nucl Med 2010;51(5): 812–818
97 Kim JH, Lee JS, Song IC, Lee DS. Comparison of segmentation-based attenuation correction methods for PET/MRI: evaluation of bone and liver standardized uptake value with oncologic PET/CT data. J Nucl Med 2012;53(12):1878–1882
98 Eiber M, Takei T, Souvatzoglou M, et al. Performance of whole-body integrated ^{18}F-FDG PET/MR in comparison to PET/CT for evaluation of malignant bone lesions. J Nucl Med 2013
99 Marshall HR, Prato FS, Deans L, Théberge J, Thompson RT, Stodilka RZ. Variable lung density consideration in attenuation correction of whole-body PET/MRI. J Nucl Med 2012;53(6):977–984